8-3-2010

Estimates for the pressure and thermal distortions of coating dies for use in design and simulation

Sneha Shetty

Estimates for the Pressure and Thermal Distortions of Coating Dies for use in Design and Simulation

Sneha Shetty

A Thesis Submitted in Partial Fulfillment of the Requirement
for Master of Science in Mechanical Engineering

Approved by:

Dr. Kenneth Ruschak – *Thesis Advisor*
Department of Chemical & Biomedical Engineering

Dr. Steven Weinstein
Department Head of Chemical & Biomedical Engineering

Dr. Edward Hensel
Department Head of Mechanical Engineering

Dr. Kathleen Lamkin-Kennard
Department of Mechanical Engineering

Dr. Hany Ghoneim
Department of Mechanical Engineering

Department of Mechanical Engineering
Kate Gleason College of Engineering
Rochester Institute of Technology
Rochester, New York 14623
August 3, 2010

Abstract

A coating die is used for distributing liquid in order to apply a uniform film on a solid surface. The fluid flowing through the die cavity can exert a pressure of up to 500,000 Pascal on the die body. This liquid pressure can distort the die and lead to a non-uniform slot opening, which in turn causes non-uniformity in the coating thickness. Distortion of the die can also occur during non-isothermal operation of the die; this is an undesired consequence of delivering liquids at a different temperature than the die itself. The distortions undergone by the die both due to liquid pressure and non-isothermal conditions should be within the manufacturing tolerances for the slot heights in order to maintain uniformity in the coating.

The deformation exhibited by a coating die due to pressure loadings is modeled both two-dimensionally and three-dimensionally. A two-dimensional model has lower computational load and is preferred for die design. For the two-dimensional analysis of a coating die, the finite element method is used to determine the deflections due to pressure loadings with a focus on slot heights. A model of low computational load is also developed based on beam theory, and its results are compared with those of the two-dimensional finite element analyses predictions. The beam model is incorporated in a die design and simulation program in which flow and slot deformations are coupled. Two-dimensional finite element analyses due to non-isothermal conditions are also performed on the coating die to give an estimate of the die deflection due to temperature variations within the die. A three-dimensional coating die with varying inner cavity area is modeled and analyzed to check its predictions with those of the two-dimensional finite element analyses and beam theory results.

In the literature reviewed, flow distribution is fully coupled to die deformation only for extrusion dies. Extrusion dies are used for extruding melted polymers of very high viscosity. Therefore, the deflections are much larger for extrusion dies than for coating dies. Mechanical adjustments can be used to manage the large deflections in the case of extrusion dies whereas coating dies have to be designed for small deflections comparable to manufacturing tolerances. This is the first time where a coupled analysis has been done for a coating die. This research provides the slot deflections for a coating die subjected to pressure loadings that vary throughout the die length. The model of flow distribution coupled with die distortion incurs low computational load and is

intended for use in design and simulation programs. Die design guidelines are developed based on examination of the die dimensions and flow parameters having the greatest effect on slot deflections.

Table of Contents

List of Figures

Nomenclature

$\bar{A}$ = Cross sectional area of the inner cavity

A = Cross sectional area of the outer cavity

A_c = Cross sectional area of the cylindrical pipe

a = Dimensionless variable for inner cavity area

b = Width of flat surface of the outer cavity

d_i = Inner cavity depth

d_o = Outer cavity depth

E = Young's Modulus of Elasticity

$\widetilde{F_t}$ = Local resultant force vector

f = Dimensionless variable for volumetric flow rate in inner cavity

g = Dimensionless variable for volumetric flow rate in outer cavity

$\bar{H}$ = Dimensionless variable for inner slot height

H' = Dimensionless variable for outer slot height

$<\bar{h}>$ = Undistorted inner slot height

$<h>$ = Undistorted outer slot height

$\bar{h}'$ = Distorted inner slot height

h' = Distorted outer slot height

$\bar{h}_m'$ = Distorted height at the middle of inner slot

h_m' = Distorted height at the middle of outer slot

I = Moment of inertia

$\tilde{\imath}$ = Unit vector in the x direction

$\tilde{\jmath}$ = Unit vector in the y direction

$\tilde{k}$ = Unit vector in the z direction

L = Cavity length

li = Width of the inner slot

l_o = Width of the outer slot

M_i = Local bending moment

$\tilde{n}_c$ =Unit vector normal to the contracting surface

$\tilde{n}_e$ =Unit vector normal to the elevating surface

$\bar{P}$ = Inner cavity and slot pressure

P = Outer cavity and slot pressure

$\bar{P}_c$ = Characteristic inner cavity and slot pressure

P_c = Characteristic outer cavity and slot pressure

p = Pressure

$\bar{Q}$ = Volumetric flow rate in the inner cavity

Q = Volumetric flow rate in the outer cavity

q = Flow rate per unit width

$<q>$ = Flow rate per unit width (perfect flow)

r = Dimensionless slot group

$\tilde{r}_i$ = Local resultant vector between the resultant force vector and the centroid of the beam

s = Dimensionless outer cavity group

T = Local thickness

To = Original thickness of the die

u = Velocity of the fluid

W_i = Width of the inner cavity

Wo = Width of the outer cavity

x_1 = Length from origin to section 1

x_2 = Length from origin to section 2

x_3 = Length from origin to section 3

x_4 = Length from origin to section 4

x_5 = Length from origin to section 5

Z = Sectional cavity length

ε = Dimensionless inner cavity group

$\frac{dP}{dx}$ = Pressure gradient

μ = Viscosity

v = Poisson's ratio

$\bar{\lambda}$ = Shape factor of the inner cavity

λ = Shape factor of the outer cavity

λ_c = Shape factor of the cylindrical pipe

θ_c = Contraction angle

θ_e = Elevation angle

ξ Dimensionless variable for cavity length

Chapter 1

I. Background

In the manufacturing process of mainly polymeric film or sheet products, coating dies are used for distributing a polymer dissolved in a solvent often with dispersed particles, in order to apply a uniform film over a solid surface. The liquid distribution geometry consists of one or two cavities running through the length of each bar (as shown in Figure 1.2) and one or two narrow slots that create high pressures in the inner cavity (referred to as back pressure). The width of the die (in the direction towards the slot exit of Figure 1.2) taken up by the cavities and slots is called the working width (Figure 1.3).

Dies may distribute more than one liquid for the purpose of coating several layers simultaneously. In that case several bars are bolted or clamped together to form a stack (Figure 1.1). A bar in a stack is in contact with pressurized liquid on both sides.

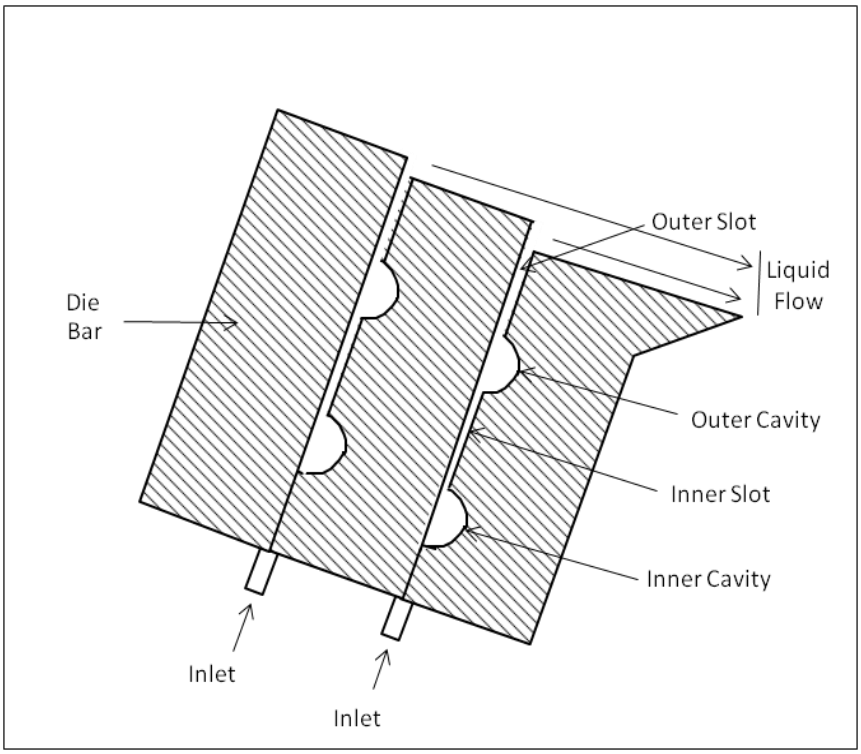

Figure 1.1: Side View of a Two Layered Coating Die

The liquid entering the die inlet flows along the length of the inner cavity (Figure 1.2). This is accomplished by choosing a cavity with a large cross-sectional area, which creates lower resistance to flow in comparison with that created by the small height of the inner slot. The inner cavity may become smaller near the ends of the die to avoid fluid flow stagnation, and it is often the case that the working width gradually decreases as well to improve performance over a range of fluid types. Flow stagnation near the cavity ends can lead to several problems including sedimentation of dispersed particulate, inefficient purging of the coating composition with solvent, and solidification of the coating composition due to a cross linking chemical reaction or to structure that can build in the liquid at low shear rates. Slot heights are on the order of 200 microns and may be manufactured to ± 0.5 micron. The outer cavity and slot combination is added to minimize the effect of slot mechanical tolerances and to increase the die's ability to uniformly deliver liquids with differing in rheology. The outer cavity also improves the flow distribution from the inner slot. The die can be regarded as a stack of bars made of high grade stainless steel having working width around 100 mm, thickness around 30 mm and die length of the order of 4 meters.

The fluid flowing through the die cavity can exert a pressure of up to 500,000 Pascal on the die body which can distort the die leading to non-uniform slot heights. Distortion of the die can also occur if liquids are delivered at a temperature different than the die itself which is maintained by water passages. The best practice to decrease the deformation of the die is to keep the coating die in the isothermal condition which does not always happen in practice. The distortions undergone by the die both due to liquid pressure and non-isothermal conditions should be within the manufacturing tolerances for the slot heights in order to maintain uniformity in the coating.

II. Die Design Fundamentals

The design of dies is complicated by disparate length scales. The cavity width and depth may be 100 times larger than the slot height, and the cavity length may be 100 or more times the cavity width and depth. The dimensions of the die and the design of the liquid passages need to be such that distortions due to pressure loading have negligible effect on

the flow distribution. Thermal distortions place a limit on temperature variations as well.

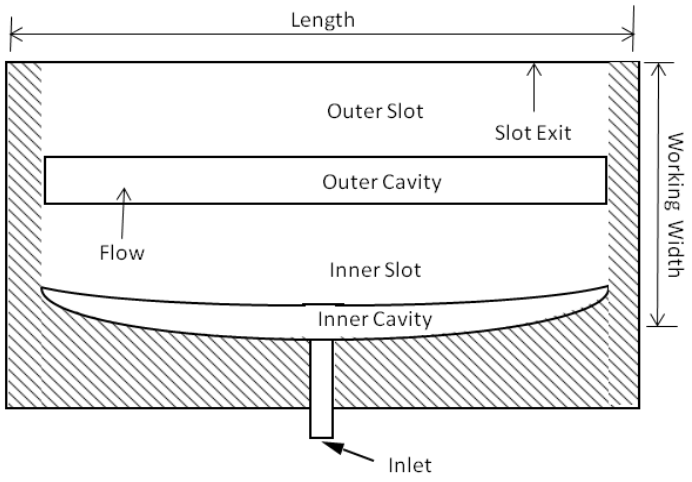

Figure 1.2: Front Section View of Coating Die

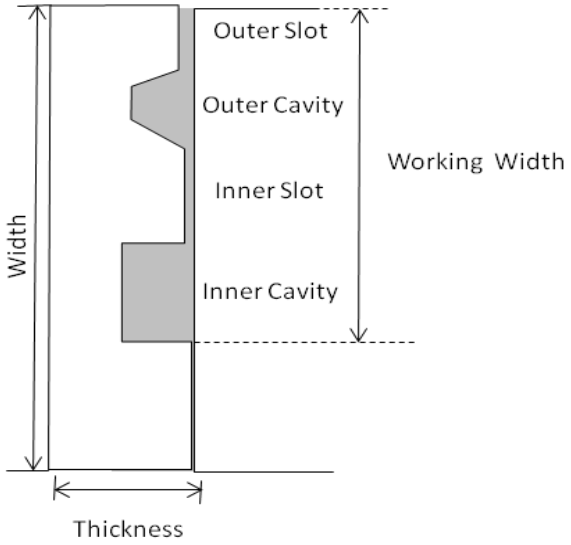

Figure 1.3: Side View of a Coating Die

Flow models are used that take advantage of the disparate length scales to simplify the governing equations. On the other hand, full finite element models have difficulty coping with the vast variation of length scales and are not suited to optimization routines. For design purposes, flow models are not coupled to pressure and thermal distortions, which are separately estimated and presumed negligible. However, flow may be coupled for simulation of a given design. Flow distribution is particularly sensitive to variations in the

height of the outer slot. Flow distribution is much less sensitive to variations in the height of the inner slot due to the dampening ability of the outer cavity on flow variations across the die length. A major benefit of a two cavity die is that the outer slot height can be larger than the inner slot height.

A coating die consisting of a tapered inner cavity is referred to as a coat-hanger shaped die and the one without taper is referred to as a T-shaped die. The outer cavity is added to dampen the flow rate variation leading to flow uniformity at the exit. The shape and aspect ratio of both the inner and outer cavities are kept constant throughout the analysis but their sizes can vary. Constant geometric cavity shapes simplifies the computation of pressure losses through what is called a shape factor. The smaller the shape factor, the higher the pressure gradient. A circular shape has the smallest shape factor. Typically, however, the inner cavity has a rectangular shape and the outer cavity a triangular or trapezoidal shape with some rounding at corners. The shape factor for the rectangular inner cavity and the trapezoidal outer cavity are less than the shape factor obtained for a circular cross section as derived in Appendix C1. The shape factors for the particular inner and outer cavities used in this work are estimated to be 0.02854 and 0.019949 respectively from a shape factor computation analysis by Dr. Steven Weinstein (private communication). The inner cavity is rectangular with an aspect ratio of 0.8, which is maintained constant as the area tapers gradually along the die length from the center towards the end. The outer cavity is trapezoidal with an expansion angle of 30^o and contraction angle of 60^o, and its aspect ratio is 0.25.

Dies for the simultaneous coating of several layers consist of a stack of bars (as shown in Figure 1.1). In that case, both sides of the bars are in contact with pressurized liquid, and as a result the pressure that produces distortion for interior bars is partially cancelled.

Chapter 2

I. Literature Review

An important requirement in the design of dies is to achieve a uniform flow rate across the die exit. This is possible by keeping the distortion within the mechanical tolerance to which the die was manufactured at great expense (slot height or slot surface flatness measurements guide hand lapping of the slot surfaces). All of the literature reviewed couples die distortion and flow models to predict flow uniformity only for extrusion dies. Extrusion dies distribute melted polymer and operate at much higher pressures where significant slot deflections always occur that are called clamshelling because of the opening of the slots. Where coupled analysis has been done, it has been iterative: flow and distortion analyses are done separately and in sequence until convergence (successive approximations). Earliest work by Pearson (1964) uses beam theory to calculate the bar distortion due to pressure and temperature variation of a flat-film extrusion die. Design guidelines for minimizing the clamshelling effect for extrusion dies have been proposed by Helmy (1988). Work on numerical simulation of slit die performance was reviewed by Sander and Pittman (1996). In this paper the interaction of melt flow and die body deflection was taken into account in a fully coupled analysis, and predictions were confirmed in experiments on a 1.2m wide high pressure die. Melt flow was treated using the Hele-Shaw approximation, and the die deflection using Mindlin thick plate theory, reducing both analyses to two dimensions with low computational load. Subsequently, Gifford (1997) developed a coupled analysis using three dimensional finite elements. Comparisons with two dimensional analyses or experimental results were not presented so the advantages provided by this significantly larger computation are unclear. However, Pittman et al. (1995) together with coupling the flow analysis with three-dimensional finite element model, also compared the coupling analysis with experimental results. Sienz et al., (2006), and Wang and Smith, (2007), use the coupled analysis to carry out an optimization routine which computes the optimal design parameters for an extrusion die keeping the distortions minimum. Secor (1997) discusses the flow distribution through internal cavities of a coating die based only on an approximate flow model; however it does not consider the effect of die deformation on the fluid flow distribution. Similarly

CFD analysis of flow in coating dies has been done by Lee, Wen and Liu (1989 and 1990) but die deformations were not considered.

II. Goal of the Research

Most of the research done so far on die deformation has been only on extrusion dies. An extrusion die is used for extruding polymer melts of very high viscosity, whereas a coating die is used for coating polymer dissolved in a solvent with viscosity less than 1 Pa-sec. The internal fluid pressures involved in the case of extrusion die is much higher than that of the coating die which results in the extrusion die distortion being greater than the distortion undergone by the coating die and typically a significant fraction of the undistorted slot height. In the case of extrusion dies mechanical die lip adjusters or choker bars can be used to correct or compensate for the distortion which aids in reducing non uniformity. These adjustments are absent in case of coating dies and hence their performance is limited by the fabrication tolerances to deliver very high uniformity. The main focus of this research is to estimate the slot distortion of a coating due to pressure and non-isothermal loadings. Die deflection can change the internal dimensions of a die which leads to alterations in the flow resulting in non uniform coating thickness. Hence the die needs to be designed so as to keep the deflection within the fabrication tolerances, and the uniformity in the flow is not affected. However, end users may use the die under conditions for which it was not designed, and as a result what happens to flow distribution when die deforms is of interest.

Chapter 3

I. Introduction

This chapter discusses the one-dimensional analysis of the coating die bar using beam theory and two-dimensional analysis of the bar using finite element method. The coating die is divided into cross-sections along the length of the bar to carry out the analyses. Each section is modeled as a beam cantilevered at the inner cavity edge and analyzed for deflection using beam theory. The beam theory results are compared with two-dimensional finite element analysis predictions obtained using ANSYS in plane strain condition. The beam theory and finite element analysis results are further compared with the three-dimensional finite element analysis predictions. This chapter also explains the two-dimensional thermal analyses performed on the die which gives an upper limit for temperature variations that can take place within a coating die.

II. One-Dimensional Analysis using Beam Theory

Estimation of slot distortion of the coating die due to pressure loading is evaluated by cross-sectioning the three-dimensional coating die along its length to obtain a beam with height T_o, width W and unit thickness. The beam is cantilevered at one end and subjected to pressure loading as shown in figure 3.1. The pressure distribution in the inner and outer cavity is constant and of the order of 500,000 and 100,000 Pascal respectively. The pressure loading in the inner cavity affects not only the bottom of the cavity but also its sides. There is a linear decrease in pressure along the width of the slots. The pressure in the inner slot decreases linearly from 500,000 to 100,000 Pascal and the pressure in the outer slot varies linearly from 100,000 to 0 Pascal along its width. The cantilevered beam is divided into six sections and each section is further divided at regular intervals for numerical computation, and the bending moment at the nodes in each section due to the applied pressure is calculated as shown in Appendix A. The Euler-Bernoulli beam equation which relates the bending moment to beam deflection and stiffness is used to obtain the deflection of the two dimensional coating die.

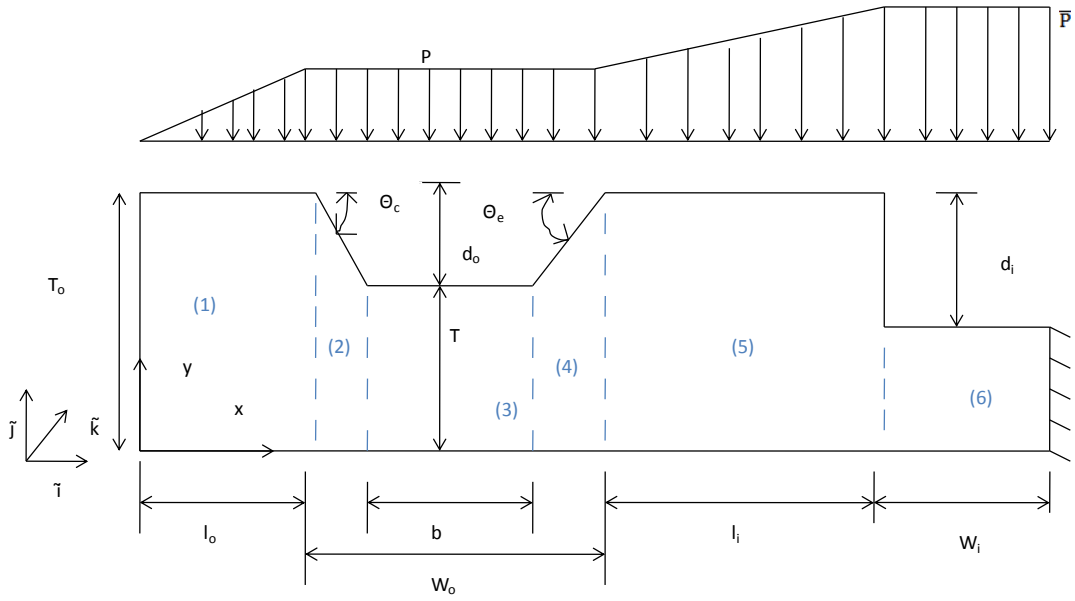

Figure 3.1: One-Dimensional Deflection Analysis using Beam Theory

The bending moments at each section is given by,

$$M_i = \tilde{k} \cdot \left(\tilde{r}_i \times \tilde{F}_i\right) \tag{3.1}$$

in which the force is computed from the pressure loading. The results obtained using the above equation are substituted into the Euler Bernoulli beam equation given below,

$$EI \frac{d^2 y_i}{dx_i^2} = M_i \tag{3.2}$$

Beams which are wide compared to their thickness cannot expand and contract laterally as much as narrow beams. This results in an increased equivalent stiffness,

$$E = \frac{E_{beam}}{1-\nu^2} \tag{3.3}$$

The moment of inertia of a rectangular beam is,

$$I = \frac{x_i T^3}{12} \tag{3.4}$$

Using the cantilevered boundary conditions, $y_o = 0$, $\frac{dy_o}{dx} = 0$ and the trapezoidal rule for the integrations, the slope and the deflection of the beam at the nodes in each section is determined.

The deflections at any point across the width of the die can be obtained in a similar way with the help of a simulation program developed using the beam theory equations (as shown in Appendix A) in Microsoft Excel. The beam modeled is programmed in a single worksheet where the lengthwise coordinate is an input. Excel's data table macro is then used to extract results for any specified number of coordinate values. The data table automatically updates the worksheet at each coordinate value and extracts the results of interest.

In the design of the coating die it is essential to keep the slot heights within the fabrication tolerances to avoid alterations in the flow which result in non uniformity in the coating thickness. In order to couple the flow with the deflection of the slots, the deformation undergone by the slots is assumed to be linear along their widths. The assumption of linear variation was checked with ANSYS calculations and found to be reasonable.

As a result of linear elasticity, the deflection at the center of the inner slot is given by,

$$\bar{h}'_m = \bar{\alpha}\bar{P} + \alpha P \qquad (3.5)$$

Similarly the average deflection at the center of the outer slot is given by,

$$h'_m = \bar{\beta}\bar{P} + \beta P \qquad (3.6)$$

The coefficients $\bar{\alpha}$, α, $\bar{\beta}$, β used to estimate the average inner and outer slot deflections along the length of the coating die are obtained using the data table function in Excel from the beam theory calculations. These coefficients depend upon the length coordinate, and so they must be computed at each of the 26 nodes used to discretize the half length of the bar. Only one half of the bar is analyzed due to symmetry.

III. Deflection Coupled with Flow Analysis

Die deflection can drastically change the slot heights of a die and can alter the flow resulting in non-uniformity in the coating thickness. Hence it is essential to couple the deflection model with the flow model to estimate the deflection at the middle of the slots, back pressure in the cavities, and flow rate variations within the slots.

The deflection and flow coupled equations for inner and outer cavities are derived by combining the continuity equations of inner and outer slots and cavities (Appendix C2) and the equation of flow in the cavities with the linearized pressure equations of the inner and outer slots as seen in Appendices C3 and C4 respectively. The coupled equations are linearized about perfect flow distribution and undeformed slots since departures of no more than a few percent are of interest. So, it is a departure from perfect flow distribution that is computed. Linear equations avoid iterative solution. The coupled dimensionless equations for the inner and outer slot are derived from the average slot deflection equations (*3.5* and *3.6*) as described in Appendix E.

As the coupled analysis has many parameters, it is convenient to use dimensionless coordinates, variables and groups of parameters (Appendix D1). The coupled equations are in dimensionless form. There are four primary variables: departures from perfect flow distribution in the inner and outer cavities, and departures from perfect slot heights. The four equations given below are from equations *(D.37), (D.41), (E.12),* and *(E.14)* derived in Appendices D and E.

Coupled dimensionless equation for inner slot,

$$\bar{H}'\left[1+3\frac{\bar{\alpha}\bar{P}_c}{<\bar{h}>}\right]+\frac{3(\bar{\alpha}+\alpha)P_c\bar{H}'}{<\bar{h}>}+\frac{(\bar{\alpha}+\alpha)P_c}{<\bar{h}>}\frac{dg'}{d\xi}+\left[\frac{\bar{\alpha}\bar{P}_c}{<\bar{h}>}+\frac{(\bar{\alpha}+\alpha)P_c}{<\bar{h}>}\right]\frac{df'}{d\xi}=\frac{(\bar{\alpha}+\alpha)}{<\bar{h}>}P_c+\frac{\bar{\alpha}}{<\bar{h}>}\bar{P}_c \quad (3.7)$$

Coupled dimensionless equation for outer slot,

$$H'\left[1+3\frac{(\bar{\beta}+\beta)P_c}{<h>}\right]+\frac{3\bar{\beta}\bar{P}_c\bar{H}'}{<h>}+\frac{(\bar{\beta}+\beta)P_c}{<h>}\frac{dg'}{d\xi}+\left[\frac{\bar{\beta}\bar{P}_c}{<h>}+\frac{(\bar{\beta}+\beta)P_c}{<h>}\right]\frac{df'}{d\xi}=\frac{(\bar{\beta}+\beta)}{<h>}P_c+\frac{\bar{\beta}}{<h>}\bar{P}_c \quad (3.8)$$

Coupled dimensionless equation for inner cavity,

$$-\frac{\epsilon\left[(1-\xi)+f'\right]}{a^2}+rsg'+\frac{d^2f'}{d\xi^2}\left[1-3\bar{H}'\right]+3\frac{d\bar{H}'}{d\xi}=0 \quad (3.9)$$

Coupled dimensionless equation for outer cavity,

$$\frac{d^2f\prime}{d\xi^2}+\frac{d^2g\prime}{d\xi^2}+3\frac{dH'}{d\xi}-sg'=0 \quad (3.10)$$

$\bar{H}'$, H' are the dimensionless variables for inner and outer slot height deflection at the center, f', g' are the dimensionless variables for the volumetric flow rates in the inner and outer cavities and ε, s, r are the dimensionless groups for inner cavity, outer cavity and slots respectively. The prime marks indicate that the slot height variations are fractions of the perfect slot height and the flow rates are fractional departures from perfect flow. Note that the equations for outer and inner cavities are coupled. In other words, the flow variation in the inner cavity effects the flow variation in the outer cavity. The coating die is divided into 26 nodes along the length of the die and the coupled dimensionless equations are solved simultaneously in Excel using the boundary condition of f' and g' is equal to 0 at the center and end of the die. The dimensionless variables obtained by solving the equations are used to compute results such as average slot deflections at the center, back pressures and flow rate variations. An advantage of spreadsheet implementation is that the equations are instantly resolved whenever an input value is changed.

IV. Two-Dimensional Finite Element Analysis due to Pressure Loading

Two-dimensional finite element analyses are carried out in order to compare their predictions with the results obtained by beam theory and also with the three-dimensional finite element analysis results. The model of the die is cantilevered and subjected to pressure loadings to determine the maximum deflection at the slot exit through finite element analysis as explained in Appendix F. The inner cavity pressure is kept constant at a value of 500,000 Pascal and it is applied to the bottom as well as to the inner cavity sides. The pressure distribution in the inner slot is linearly varied from 500,000 to 100,000 Pascal. The outer cavity is subjected to a uniform pressure loading of 100,000 Pascal. The outer slot pressure is decreased from 100,000 Pascal to no pressure at the slot exit. These pressure values are arbitrary for the purpose of comparisons. The two-dimensional finite element analyses are carried out at various cross-sections along the length of the die in order to compare the maximum deflection occurring at each section with the beam theory and three-dimensional finite element analysis predictions.

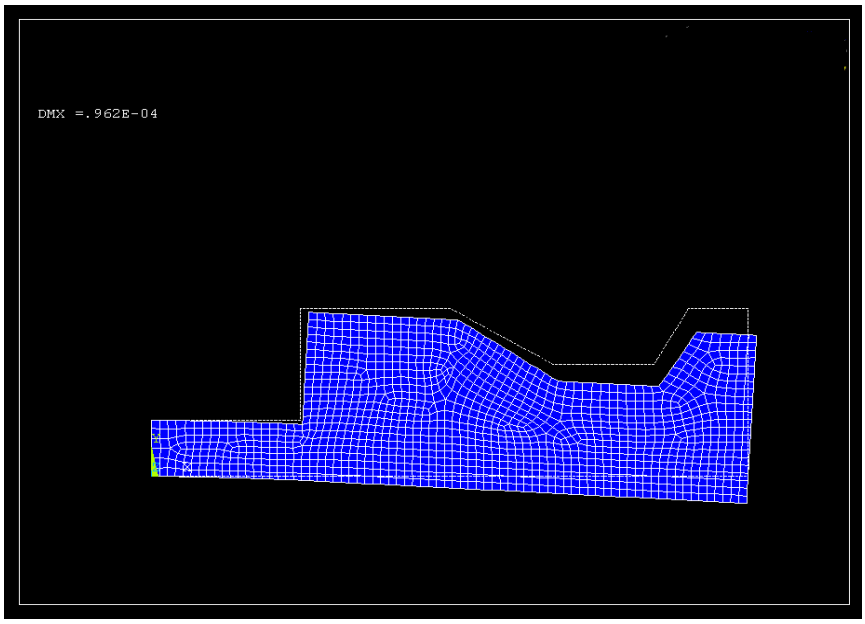

Figure 3.2: Two-Dimensional Finite Element Analysis at the Die Center (Z=0mm)

Figure 3.2 shows the deformed and the undeformed edges of the die at the center due to pressure loading. The maximum deflection of 0.0962 mm occurs at the outer slot exit. The two-dimensional finite element analysis also confirms our assumption of considering the deflections of the slots to be linear in coupled equations. This can be seen from the graph shown below. The assumption is particularly good for the critical outer slot.

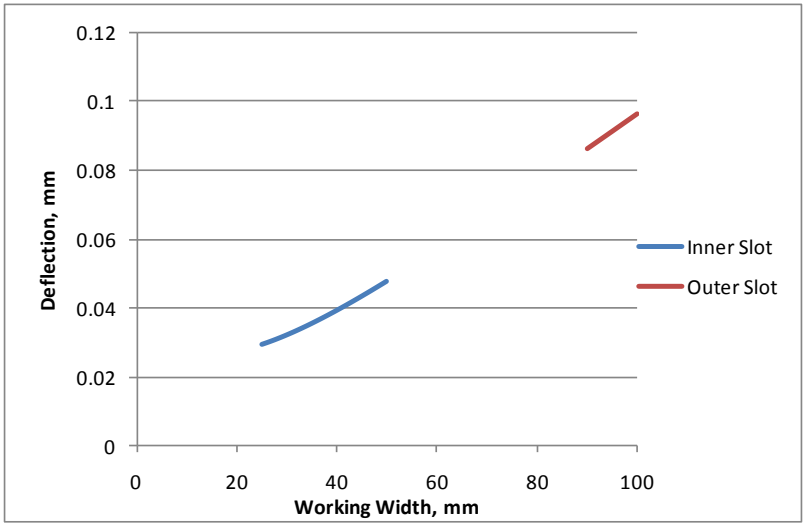

Figure 3.3: Slot Deflections along the Working Width at the Die Centre (Z=0mm)

V. Two-Dimensional Finite Element Analysis due to Non-Isothermal Loading

The distortion of the coating die also takes place when the die is at a temperature different than that of the coating fluid. Two-dimensional finite element analyses of the coating die are carried out to evaluate the temperatures close to which the die shows approximately the same amount of deflection as the coating die subjected to pressure loading (Appendix G). For the purpose of two-dimensional thermal analysis, a die model similar to the pressure loading analysis is considered which is insulated on cantilevered edge and the end of the die width. The bottom surface is a constant 20^{o}C, and the top surface is the temperature of the liquid which is set to different values. The die is cantilevered near the inner cavity edge and the thermal loadings as explained above are applied to estimate the deflections undergone by the die when subject to non-isothermal loading alone. Figure 3.4 shows the nodal temperature distribution within the die when the fluid temperature is 22^{o}C and the ambient temperature is kept at 20^{o}C. The hotter liquid opens the slots.

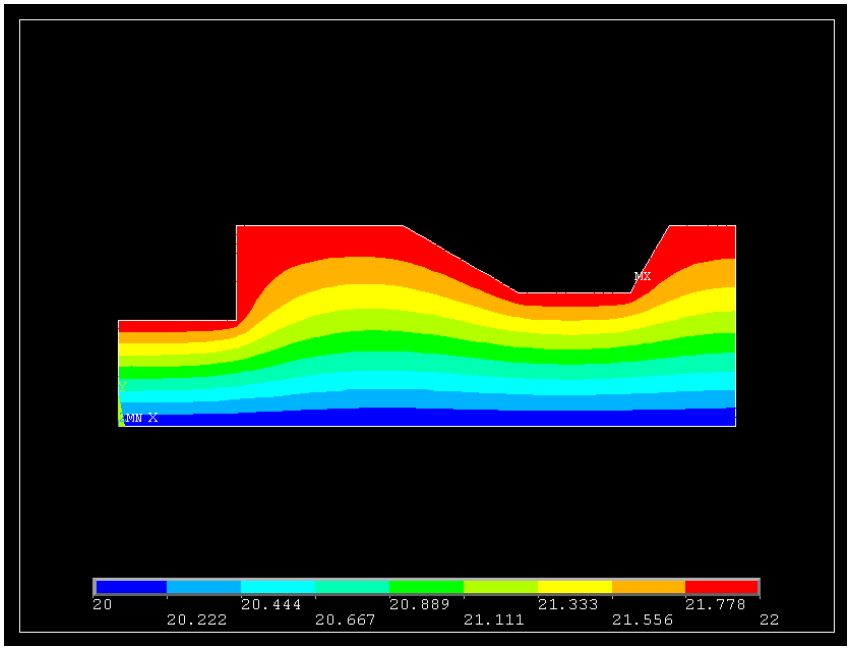

Figure 3.4: Nodal Temperature Distribution at the Die End (Z=1000mm)

Thermal analyses on the coating die were carried out to estimate the maximum slot deflection for different liquid temperatures in order to determine the sensitivity to

operating temperatures. It can be seen from the graph below that deflection varies linearly with change in temperature.

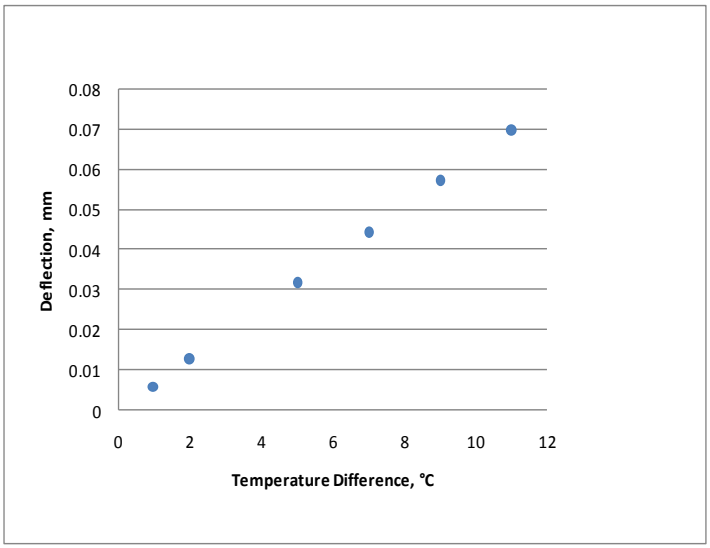

Figure 3.5: Maximum Deflection at die end (Z=1000mm) Vs Temperature Difference

The maximum deflections undergone by the coating die when the fluid temperature is 22^{o}C and ambient temperature is 20^{o}C at the die length end (z=1000 mm) is 0.0127 mm (Figure 3.6) which is close to the pressure loading deflection of 0.0122 mm calculated using beam theory.

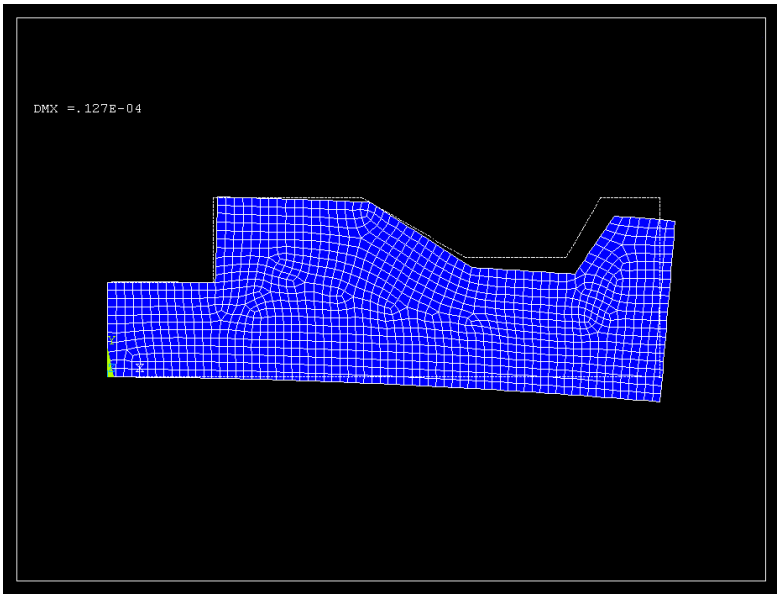

Figure 3.6: Two-Dimensional Finite Element Analysis at the die end (Z=1000mm)

Theoretically, the minimum deflection of the die would occur under isothermal conditions. However, in practice it is not possible to maintain a strictly isothermal condition during the coating process. The knowledge of the amount deflection undergone by the die for a particular change in temperature gives an upper limit to the temperature change that can take place within the die body. Although, water jackets are provided within the die body in order to achieve an isothermal condition the temperature of the feed stream may not match perfectly. Therefore, the sensitivity of a design to temperature differences is of considerable interest.

VI. Three-Dimensional Modeling and Analysis of a Coating Die

The coating die is modeled three dimensionally with linearly varying inner cavity area, referred to as coat-hanger which results in the reduction of its working width but with constant aspect ratio along the die length using Pro-Engineer Wildfire 4.0 as discussed in Appendix H1.

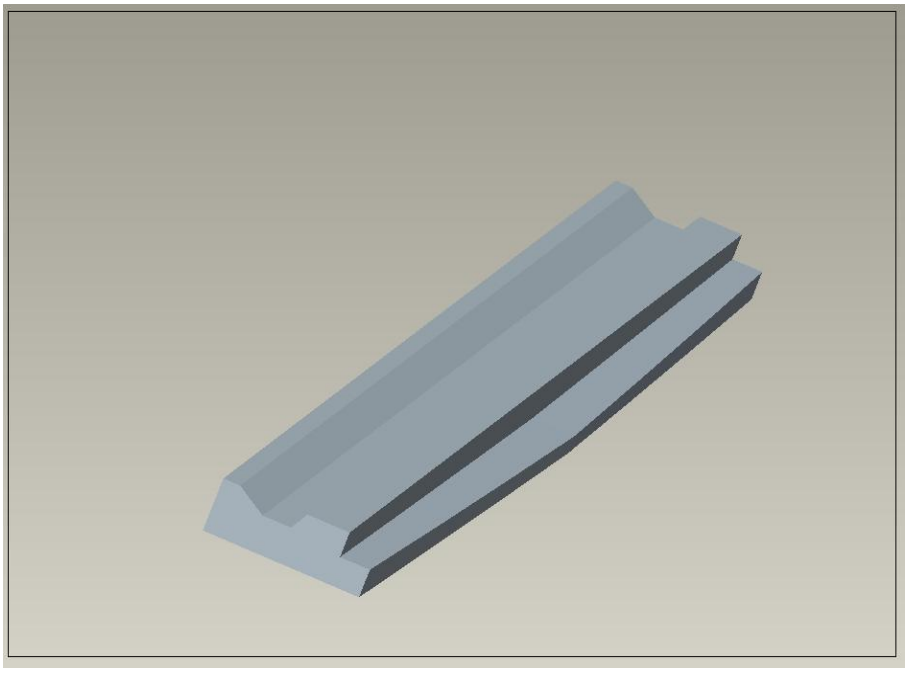

Figure 3.7: Three-Dimensional Model of a Tapered Coating Die

The three-dimensional model is saved in Initial Graphics Exchange Specification (IGES) format in order to export the part file into ANSYS 12.0. The three-dimensional finite

element analysis of the coating die is carried out on the imported model as explained in Appendix H2. Only one half of the die is considered for analysis due to its symmetric geometry. The pressure distribution for three-dimensional analysis is maintained uniform over the cavities and slots for the ease of applying the pressure loading in three dimensions. The pressure applied on the inner and outer cavities is 500,000 and 100,000 Pascal respectively and the average pressure along the inner and outer slot is 300,000and 50,000 Pascal respectively. The result obtained by this analysis is compared with the two-dimensional analysis results with the same pressure distribution applied on the three dimensional model.

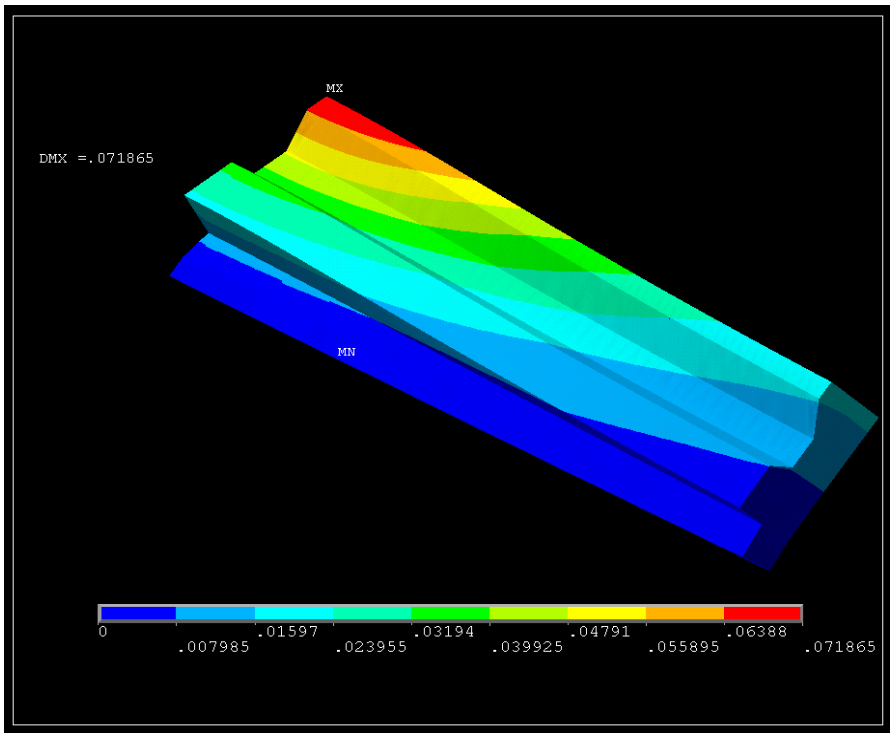

Figure 3.8: Three-Dimensional Finite Element Analysis of the Tapered Coating Die

The maximum deflection undergone by the coating die during the three-dimensional analysis is 0.071865 mm at the center of the die and end of the outer slot and the maximum deflection of the die obtained from two-dimensional analysis for the same pressure loading using finite element analysis is 0.104 mm at the same location. Figure 3.9 shows the contour plot of the nodal deflections at the end of the outer slot along one half of the die length. The maximum deflection is marked by the red color and occurs at

the outer slot and at the center of the die length. The region where the die is cantilevered is marked by the blue color and exhibits no deflection. It can also be observed that the deflection at the die exit gradually decreases from the die center along the length of the die. This behavior is expected since the end of the bar is much stiffer than the center as a result of the shorter work width and shallower inner cavity.

VII. Results

The maximum deflection which takes place at the die center near the outer slot exit obtained from beam theory is 0.08265274 mm. The two-dimensional finite element analysis predicts a maximum deflection of 0.0962 mm. The ANSYS gives a higher deflection values when compared to beam theory results.

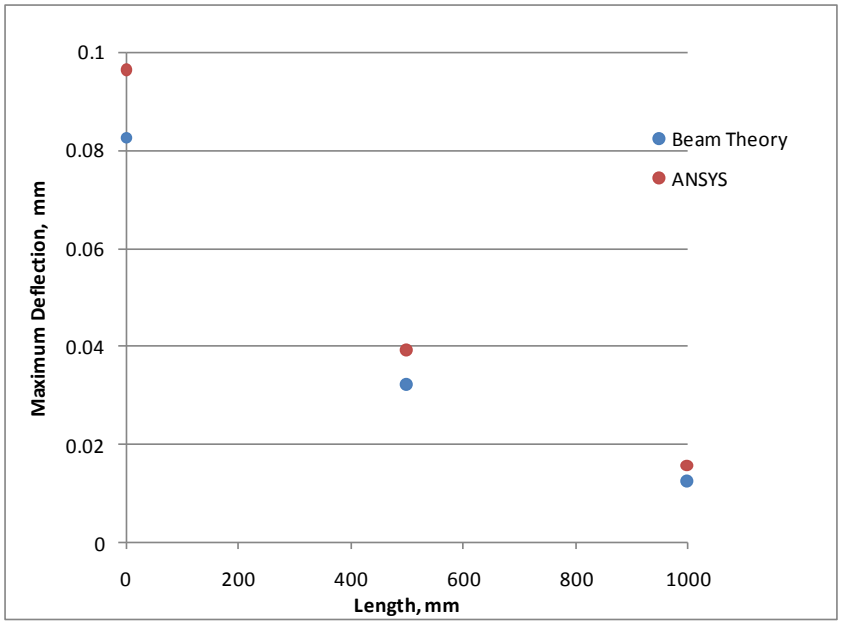

Figure 3.9: Maximum Deflection at Sections along the Die Length

The three-dimensional analysis carried out with constant pressure loading along the width of the cavities and slots is compared with two-dimensional finite element analysis predictions with the same pressure loading. From the graph below, it is observed that the two-dimensional finite element analysis over predicts the deflection at the center of the die. The two-dimensional finite element analysis predictions show a close agreement with the three-dimensional analysis results as we move along the die length.

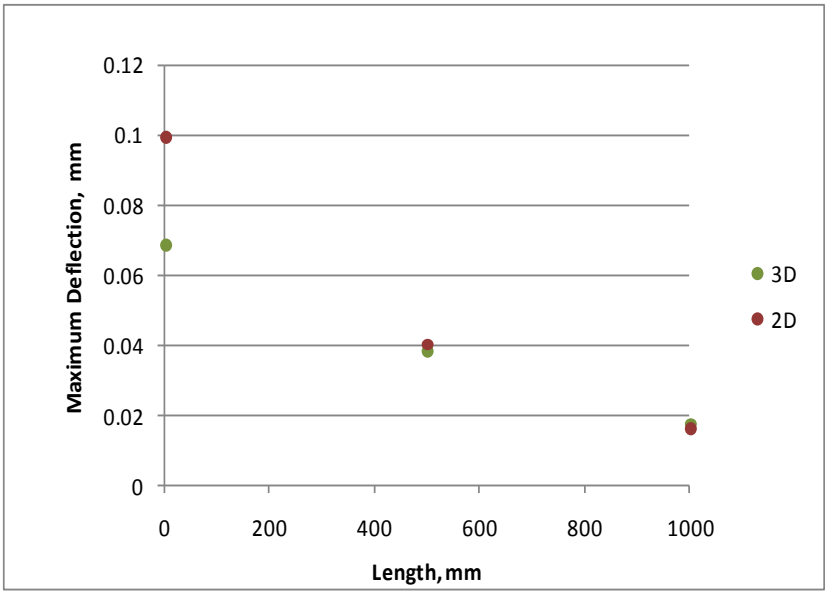

Figure 3.10: Maximum Deflection at Sections along the Die Length

The three-dimensional analysis is carried out with a pressure loading higher than that used in beam theory. Hence the three-dimensional coating die will exhibit a maximum deflection greater than the actual deflection. It has been observed that maximum deflection in a coating die takes place at the die center. The graph below shows that the beam theory over predicts the maximum deflection occurring at the die center.

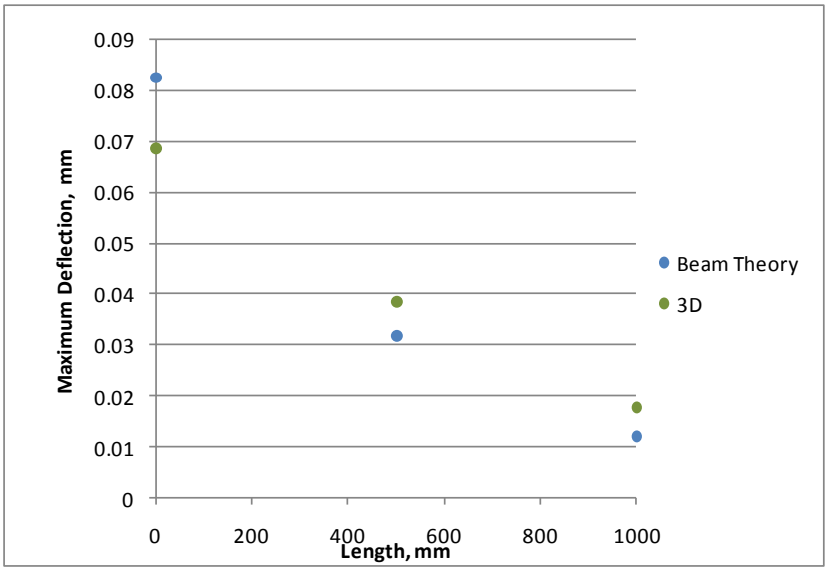

Figure 3.11: Maximum Deflection at Sections along the Die Length

Based on this data dies can be designed keeping the deflection obtained by the program as an upper limit.

The simulation program couples the deflection and the flow equations to obtain the following results along the length of the coating die.

1. Deflections undergone at the middle of inner and outer slots

   The graph below shows the slot deflections at the middle. The deflection of the slots is maximum at the die center and it gradually decreases as we move along the die length.

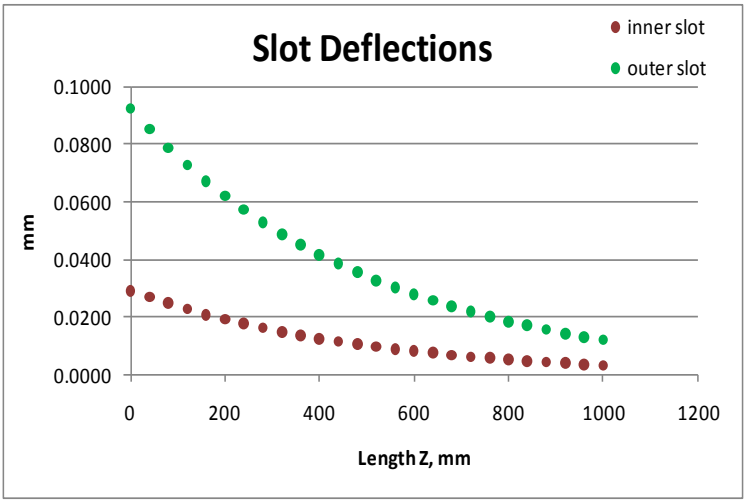

Figure 3.12: Slot Deflections along the Die Length

2. Flow rate variations in the slots.

   The coupled analysis estimates the flow rate variation within the slots due to its deflection. Since the slot deflection is maximum at the die center, the flow rate variation in the slots is also maximum at this section. The variation in flow gradually decreases as seen from the graph below due to the decrease in slot deflection. Hence, larger the slot deflection, greater will be the flow rate variation. Therefore it is essential to keep the slot deflections at a minimum in order to obtain a uniform flow.

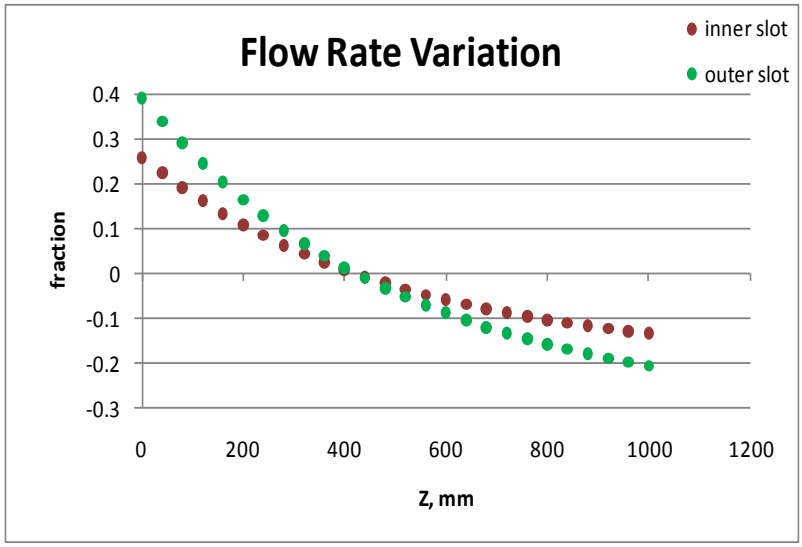

Figure 3.13: Flow Rate Variation Ratio along the Die Length

3. Back pressures in the cavities due to the deflection in the slot heights

   The narrow slot heights create a high pressure in the cavities which is referred to as the back pressure. The coupled analysis estimates the back pressure created in the cavities due to the slot deflection. From the graph below we can see that, the back pressure in the cavities is lower at the die center where the slot deflection is maximum. The cavity pressure decreases slightly as we move along the die length due to reduced slot deflection.

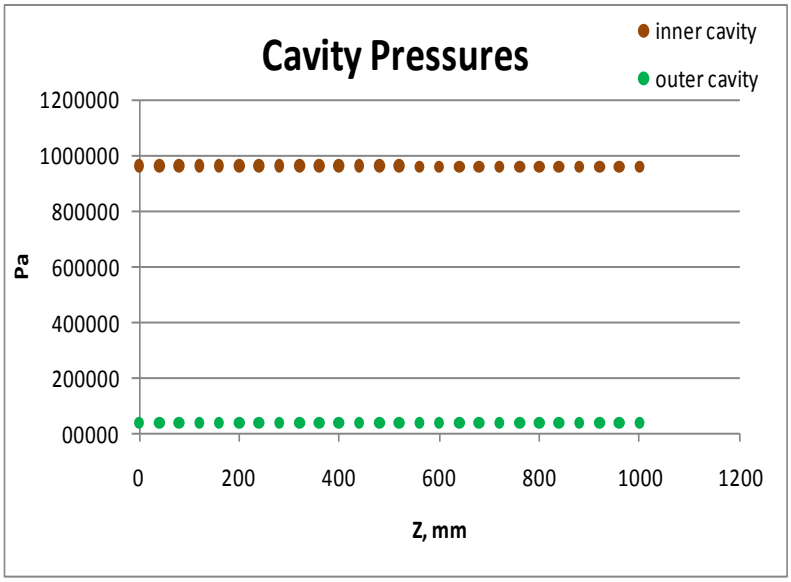

Figure 3.14: Cavity Pressures along the Die Length

Chapter 4

I. Design Guidelines

Die deflection in a coat-hanger type coating die is one of the areas that has not been addressed by die designers. When a die deflects, the inner and outer slot heights will increase substantially more in the middle of the die than at the ends. The result is that the die which was designed for uniform flow will now exhibit heavy flow in the middle. The main objective of the coating process is to obtain uniformity in coating film thickness. The simulation program based on beam theory is developed to predict the deflection at the slot centers along the flow passages and across the length of the coating die. It also estimates the back pressure and the flow rate variations in the cavities due to the changes in the slot heights. The program treats the die as a non-uniformly loaded beam with varying cross sections. The input information to the model is:

1. The shape and the thickness of the die body
2. Average flow rate per unit width

The program calculates the inner and outer slot deflections at their centers, back pressure and the flow rate variation ratios in the cavities along the length of the die. An optimization routine is carried out using the Solver function, a general purpose optimization routine that is available within Excel as an add-in, to determine various geometric parameters for the die design which would result in uniform coating thickness by reducing deflection and controlling the flow rates. The die dimensions that are found to have greatest effect on the deflections are:

1. Thickness of the die body

   Increasing the thickness of the die reduces the inner and outer slot deflections and peak to peak flow rate variation ratios as seen in figures 4.1 and 4.2. However, end users want the bar to have minimum weight and cost. Increasing the thickness of the bar results in an increase in material cost and weight. Hence a bar with appropriate thickness can be chosen by the user which strikes a good balance between the cost, weight and the performance of the die. This can be estimated from the simulation

program developed in Excel. The thickness of the bar is also a consideration while stacking bars used for multi layered coating because the overall size and weight of the die is affected.

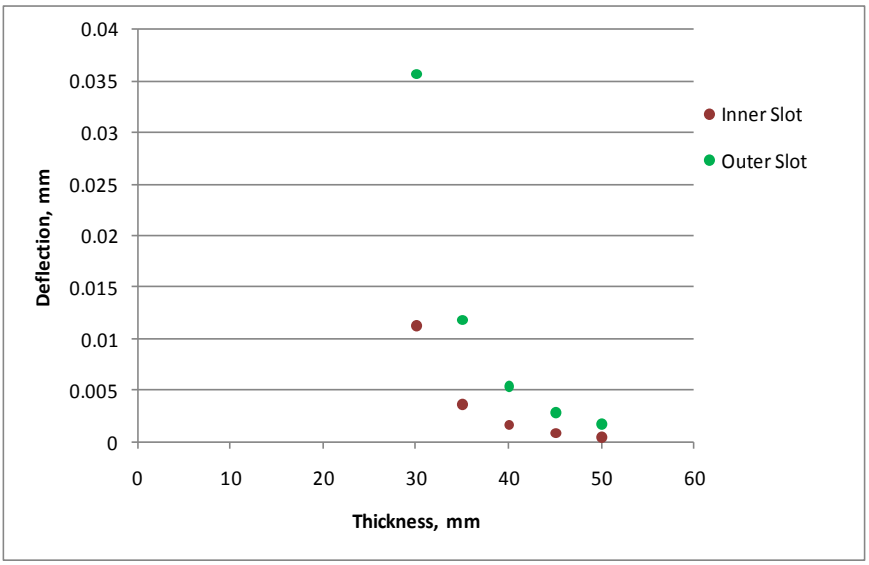

Figure 4.1: Slot Deflections Vs Thickness of the Coating Die

2. Working width

The width of the cavities and slots makes up the working width of the coating die. In a coat hanger type die the working width gradually decreases from the center due to the tapering of the inner cavity area along the length of the die. The optimization routine using Solver in Excel indicates that reducing the working width minimizes the slot deflections as seen in figure 4.3. This makes sense because a longer working width acts as a lever which results in an increase in the slot deflection leading to non uniformity in the flow.

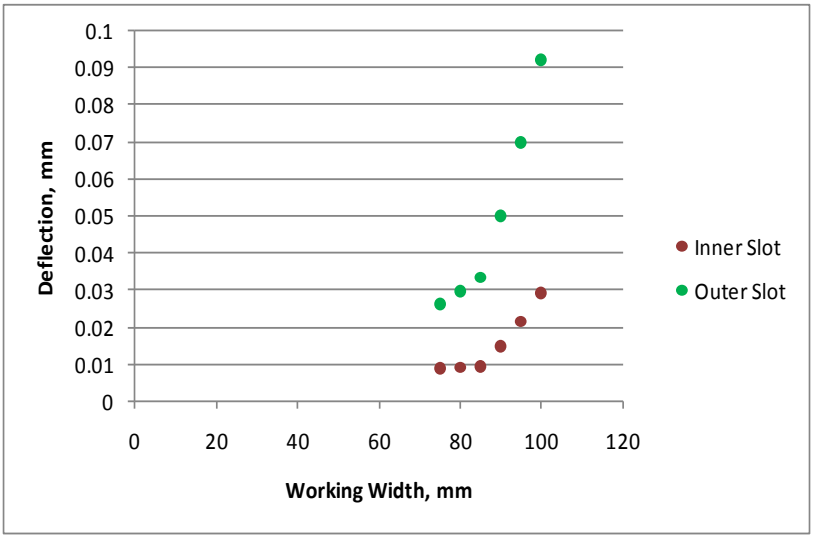

Figure 4.2: Slot Deflection Vs Working Width of the Coating Die

3. Linear reduction in the area of the inner cavity

The Solver optimizes deflection at the slot centers by removing the linear taper on the coating die, by keeping the area of the inner cavity constant throughout the length of the coating die. However in practice, the inner cavity is made smaller at the ends to avoid the following occurrences:

a. Sedimentation of dispersed particulate
b. Solidification of Non-Newtonian liquids which takes place due to decrease in velocity and shear rate
c. Solidification of liquids undergoing a cross linking reaction
d. For the ease of purging the coating liquid with solvent at the ends of the die

Figure 4.4 shows a decrease in the deflection at the center of the slots as the taper is reduced at the die center

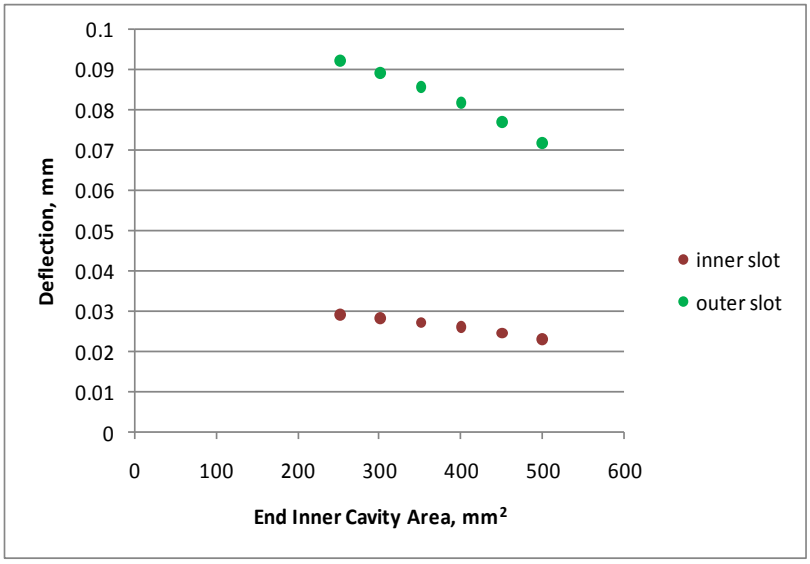

Figure 4.3: Slot Deflections Vs End Inner Cavity Area

Minimization of the deflection at the middle of the slots induces an increase in the back pressure due to the slots. The graph below shows the change in back pressure resulting from varying the outer slot height and keeping the inner slot height constant. Increasing the height of the outer slot reduces the back pressure exerted on the cavities considerably with a small change in the back pressure exerted due to inner slot height.

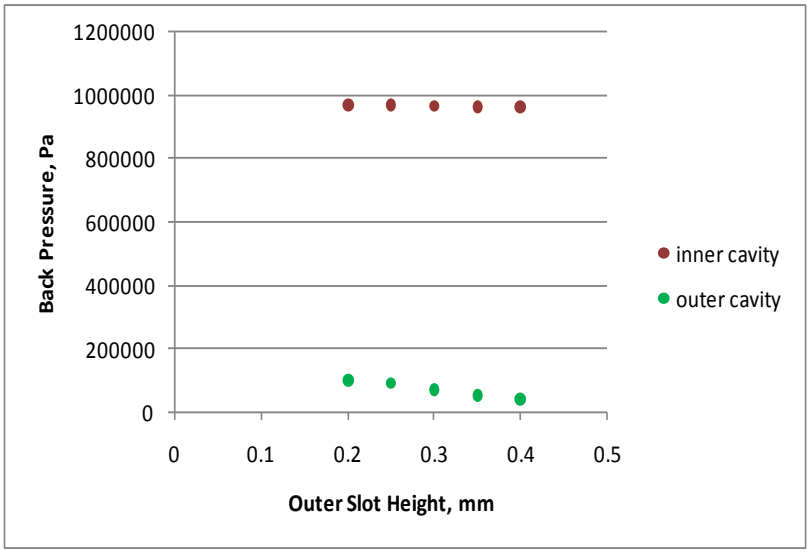

Figure 4.4: Back Pressure in the Cavities Vs Outer Slot Height

To obtain a uniform flow across the length of the coating die the back pressure developed due to the slot heights needs to be minimized. Hence, during the design of the coating die the height of the inner and outer slots should be chosen appropriately which reduces the back pressure. For a uniform flow, the outer slot height is kept larger than the inner slot height.

Summary of design guidelines:

- increase bar thickness to a maximum (consistent with cost and weight constraints)
- reduce working width to a minimum
- minimize any inner cavity taper (present for other reasons)
- maximize slot heights to reduce back pressure

The advantage of the die model developed is that the Solver optimization routine can be used to minimize flow non-uniformity subject to constraints. This approach is very efficient compared to trial and error.

II. Conclusions and Recommendations

The two-dimensional beam theory is a low load computational model which couples both the deflection and flow to give an estimate of the deflection and flow rate variations. The estimates obtained from the simulation program can be used by applying a factor of safety by the die designers in designing various die parameters for coating process involving liquids with different flow rates and viscosities.

For future work, it is recommended to conduct the three dimensional finite element analysis with the pressure loading similar to the beam theory loading in order to get a much more accurate comparison between the beam theory and three dimensional finite element results. From the thermal analyses conducted on the two dimensional die, it can be concluded that small temperature variation within the die, of the order of a couple of degree Celsius, can increase the deflection. Hence for future work it is recommended to include thermal variation in the die design and simulation process.

The optimization process performed on the simulation program suggests certain guidelines to minimize the die deflection. Some of the guidelines may not satisfy the

practical problems faced by the die designer. For example, increasing the thickness of the die reduces the maximum deflection; however increasing the thickness of the die also increases the cost and weight of the die. Design guidelines also suggest that reducing the inner cavity taper minimizes the deflection undergone by the die. The inner cavity is tapered to avoid problems such as fluid flow stagnation, sedimentation, solidification of Non-Newtonian liquids. A tapered inner cavity also helps in purging at the ends. Therefore during the design phase the design guidelines need to be balanced against the cost, machining capabilities and practical conditions to enhance coating uniformity. Since die design is an optimization problem, a model of low computational load that can be combined with an optimization routine like Solver can be very useful.

References

Q. Wang, and D. E. Smith, “Analysis of the fluid-structure interaction in the optimization-based design of polymer sheeting dies,” Journal of Applied Polymer Science, vol. 103, pp. 3994-4004, 2007.

T. Q. Wu, B. Jiang, S. H. Xu, and N. B. Huang, “Three-dimensional nonisothermal simulation of a coat hanger die,” Journal of Applied Polymer Science, vol. 101, pp. 2911-2918, 2006.

J. Sienz, S. J. Bates, and J. F. T. Pittman, “Flow restrictor design for extrusion slit dies for a range of materials: Simulation and comparison of optimization techniques,” Finite Elements in Analysis and Design, pp.430-453, 2006.

Y. H. Huang, C. R. Gentle, and J. B. Hull, “A comprehensive 3-D analysis of polymer melt flow in slit extrusion dies,” Advances in Polymer Technology, vol. 23, pp. 111-124, 2004.

S. J. Bates, J. F. T. Pittman, J. Sienz, and D. S. Langley, “Enhancing slit die performance by optimization of restrictor profiles,” Polymer Engineering and Science, vol. 43, pp. 1500-1511, 2003.

W. A. Gifford, “A three-dimensional analysis of the effect of die body deflection in the design of extrusion dies,” Polymer Engineering and Science, vol. 38, pp. 1729-1739, 1998.

W. A. Gifford, “A three-dimensional analysis of coextrusion,” Polymer Engineering and Science, vol. 37, pp. 315-320, 1997.

R. B. Secor, “Analysis and design of internal coating die cavities,” in Liquid Film Coating, pp. 269-298, 1997.

W. A. Gifford, “The use of three-dimensional computational fluid dynamics in the design of extrusion dies,” Journal of Reinforced Plastics and Composites, vol. 16, pp. 661-674, 1997.

R. Sander and J. F. T. Pittman, “Simulation of slit dies in operation including the interaction between melt pressure and die deflection,” Polymer Engineering and Science, vol. 36, pp. 1972-1989, 1996.

J. F. T. Pittman, R. Sander, W. Schuler, H. Pick, G. Martin, and W. Stannek, "Mechanical effects in extrusion :Slit Dies – Experimental and numerical determination of the die body deflection," International Polymer Processing, vol. 10, pp. 137-147, 1995.

F. Durst, U. Lange, and H. Raszillier, "Minimization and control of random effects on film thickness uniformity by optimized design of coating die internals," The Mechanics of thin coating dies, pp. 85-94, 1995.

F. Durst, U. Lange, and H. Raszillier, "Optimization of distribution chambers of coating facilities," Chemical Engineering Science, vol. 49, pp. 161-170, 1994.

P. Y. Wu, T. J. Liu, and H. M. Chang, "Design of an extrusion die with a variable choker bar," Journal of Applied Polymer Science, vol. 51, pp. 1005-1014, 1994.

Lee KY, Wen SH and Liu TJ, "Vortex formation in a dual-cavity coat-hanger die," Polymer Engineering and Science, pp. 1220-1227, 1990.

Lee KY, Liu TJ, "Design and Analysis of a dual-cavity coat-hanger die," Polymer Engineering and Science, pp. 1066-1075, 1989.

H. Helmy, "Recent developments in flat film and sheet dies," Journal of Plastic Film & Sheeting, vol. 4, pp. 193-213, 1988.

H. Helmy, "Aspects of the design of coathanger dies for cast film and sheet applications," Advances in Polymer Technology, vol. 7, pp. 59-69, 1987.

J. R. A. Pearson, "Non-Newtonian flow and die design-Part-IV," Transactions and Journal, vol. 32, pp. 239-244, 1964.

J. R. A. Pearson, "Non-Newtonian flow and die design-Part-III," Transactions and Journal, vol. 31, pp. 125-131, 1963.

J. R. A. Pearson, "Non-Newtonian flow and die design-Part-I and Part-II," Transactions and Journal, vol. 30, pp. 230-239, 1962.

J. F. Carley, "Flow of melts in crosshead-slit dies; Criteria for die design," Journal of Applied Physics, vol. 25, No. 9, 1954.

Appendix A

Bending Moments of a One- Dimensional Beam Model

This appendix shows the mathematical derivations of obtaining the bending moments at each of the six sections of the two dimensional beam (Figure 3.1).

Bending Moment at Section (1):

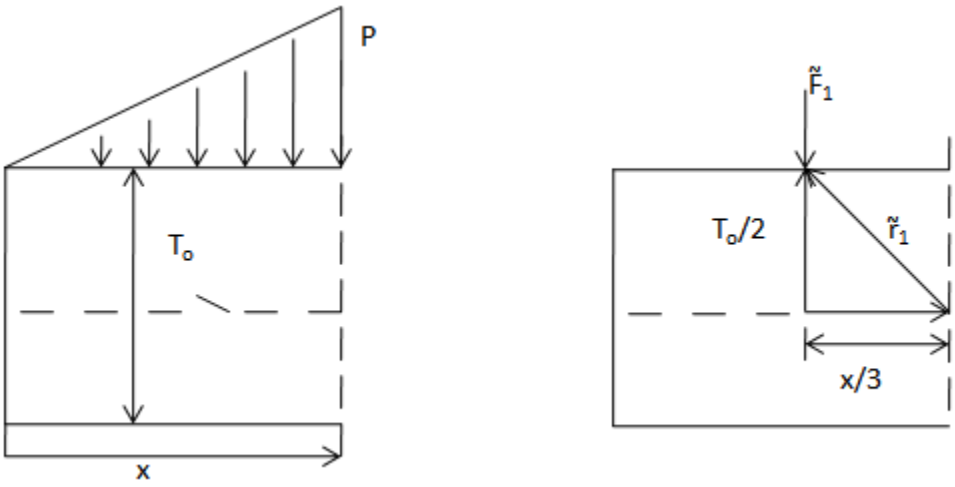

Figure A.1: Bending Moment at Section (1)

Resultant force vector, $$\tilde{F_1} = -\frac{1}{2}\, px\tilde{j} \qquad (A.1)$$

For uniformly varying load $$p = \frac{P}{l_o}x \qquad (A.2)$$

Substituting equation *(A.2)* in *(A.1)* we have,

$$\tilde{F_1} = -\frac{1}{2}\,\frac{P}{l_o}x^2\tilde{j} \qquad (A.3)$$

Resultant vector between the resultant force vector and the centroid of the beam,

$$\tilde{r_1} = -\frac{x}{3}\tilde{\imath} + \frac{T_o}{2}\tilde{j} \qquad (A.4)$$

Bending Moment,

$$M_1 = \tilde{k} \cdot (\tilde{r}_1 \times \tilde{F}_1) \qquad (A.5)$$

Substituting equation *(A.3) and (A.4)* in *(A.5)* we have,

$$M_{1=} \frac{Px^3}{6l_0} \qquad (A.6)$$

Considering any Section after Section (1):

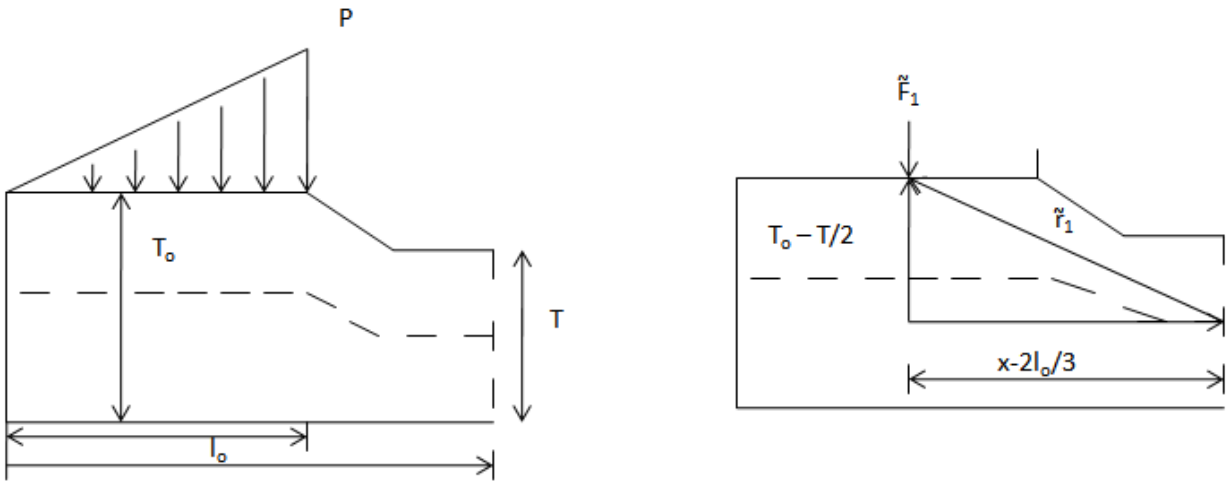

Figure A.2: Bending Moment after Section (1)

Resultant force vector, $$\tilde{F}_1 = -\frac{1}{2} P l_o \tilde{j} \qquad (A.7)$$

Resultant vector between the resultant force vector and the centroid of the beam,

$$\tilde{r}_1 = -\left(x - \frac{2}{3} l_o\right)\tilde{\imath} + \left(T_0 - \frac{T}{2}\right)\tilde{\jmath} \qquad (A.8)$$

Bending Moment,

$$M_1 = \tilde{k} \cdot (\tilde{r}_1 \times \tilde{F}_1) \qquad (A.9)$$

Substituting equation *(A.7) and (A.8)* in *(A.9)* we have,

$$M_{1=} P l_o \left(\frac{x}{2} - \frac{l_0}{3}\right) \qquad (A.10)$$

Bending Moment at Section (2):

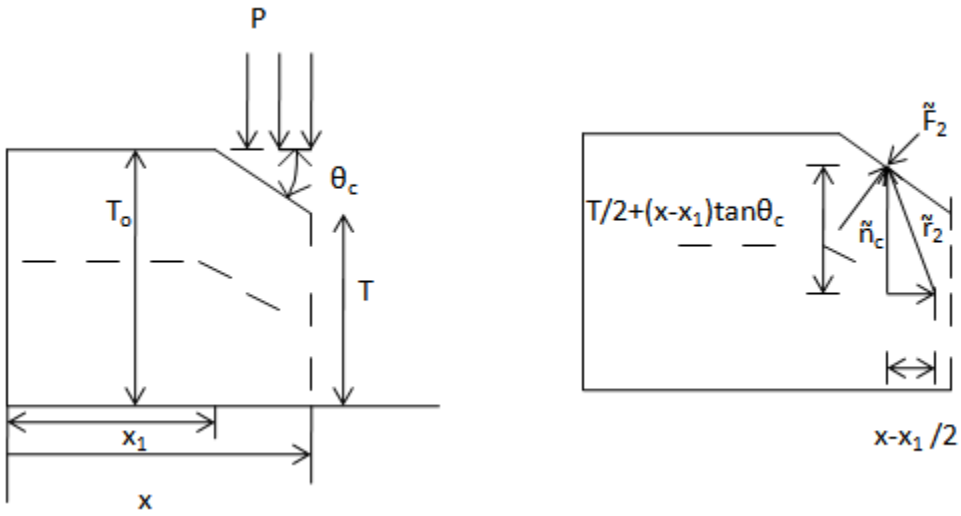

Figure A.3: Bending Moment at Section (2)

Resultant force vector, $$\tilde{F}_2 = -P\frac{(x-x_1)}{\cos\theta_c}\tilde{n}_c \qquad (A.11)$$

Unit vector normal to the contracting surface is given by,

$$\tilde{n}_c = \cos\theta_c\,\tilde{j} + \sin\theta_c\tilde{\imath} \qquad (A.12)$$

Substituting equation *(A.12)* in *(A.11)*,

$$\tilde{F}_2 = -P\frac{(x-x_1)}{\cos\theta_c}(\cos\theta_c\,\tilde{j} + \sin\theta_c\tilde{\imath}) \qquad (A.13)$$

Resultant vector between the resultant force vector and the centroid of the beam,

$$\tilde{r}_2 = -\left(\frac{x-x_1}{2}\right)\tilde{\imath} + \left\{T_o - \frac{T}{2} - \left[\left(\frac{x-x_1}{2}\right)\tan\theta_c\right]\right\}\tilde{j} \qquad (A.14)$$

Bending Moment,

$$M_2 = \tilde{k}\cdot\left(\tilde{r}_2 \times \tilde{F}_2\right) \qquad (A.15)$$

Substituting equation *(A.13) and (A.14)* in *(A.15)* we have,

$$M_{2=}\frac{1}{2}P(x-x_1)[(x-x_1)+T_o\tan\theta_c] \qquad (A.16)$$

Considering any Section after Section (2):

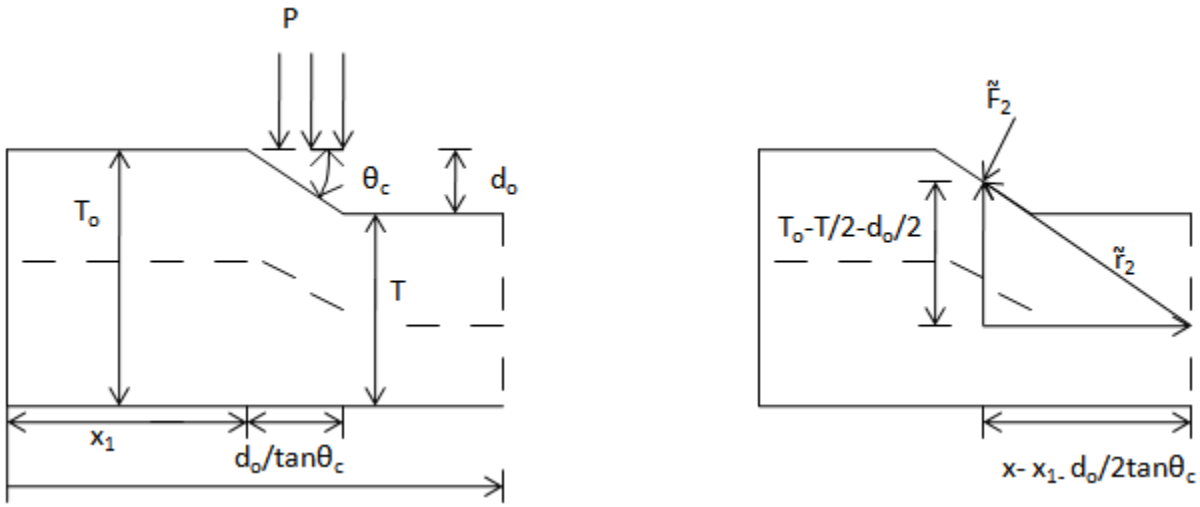

Figure A.4: Bending Moment after Section (2)

Resultant force vector, $$\tilde{F}_2 = -P\frac{d_o}{\sin\theta_c}(\cos\theta_c\,\tilde{j} + \sin\theta_c\tilde{i}) \qquad (A.17)$$

Resultant vector between the resultant force vector and the centroid of the beam,

$$\tilde{r}_2 = -\left[x - \left(x_1 + \frac{1}{2}\frac{d_o}{\tan\theta_c}\right)\right]\tilde{\imath} + \left\{T_o - \left(\frac{d_o}{2} + \frac{T}{2}\right)\right\}\tilde{\jmath} \qquad (A.18)$$

Bending Moment,

$$M_2 = \tilde{k}\cdot\left(\tilde{r}_2 \times \tilde{F}_2\right) \qquad (A.19)$$

Substituting equation *(A.17) and (A.18)* in *(A.19)* we have,

$$M_{2=}\frac{1}{2}P(x - x_1)[(x - x_1) + T_o\tan\theta_c] \qquad (A.20)$$

Bending Moment at Section (3):

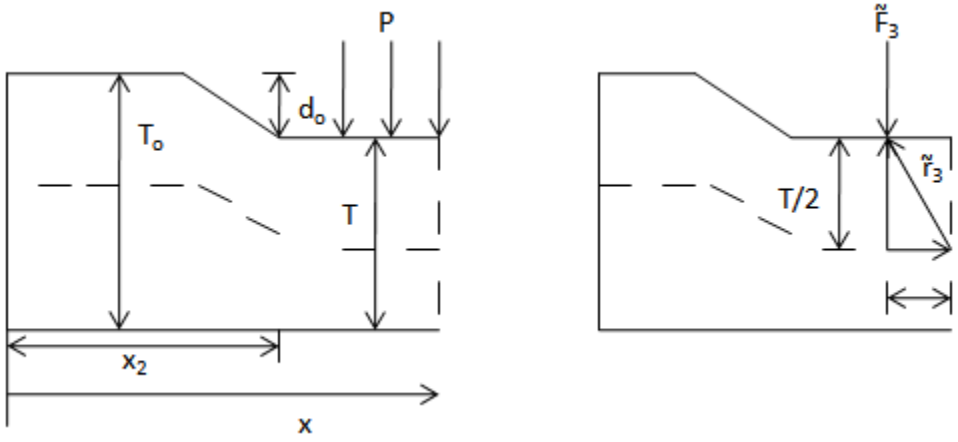

Figure 4.5: Bending Moment at Section (3)

Resultant force vector, $$\tilde{F}_3 = -P(x - x_2)\tilde{j} \quad (A.21)$$

Resultant vector between the resultant force vector and the centroid of the beam,

$$\tilde{r}_3 = -\frac{1}{2}(x - x_2)\tilde{\imath} + \frac{T}{2}\tilde{j} \quad (A.22)$$

Bending Moment,

$$M_3 = \tilde{k} \cdot (\tilde{r}_3 \times \tilde{F}_3) \quad (A.23)$$

Substituting equation *(A.21) and (A.22)* in *(A.23)* we have,

$$M_{3=} \frac{P}{2}(x - x_2)^2 \quad (A.24)$$

Considering any Section after Section (3):

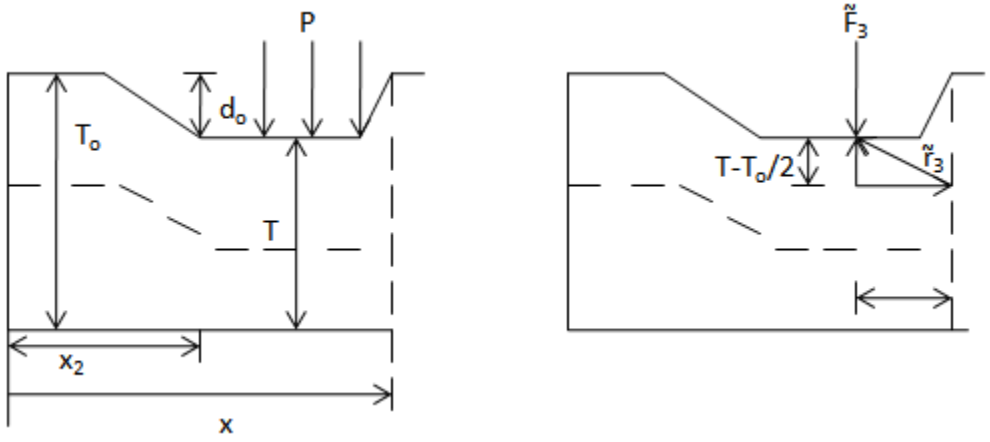

Figure 4.6: Bending Moment after Section (3)

Resultant force vector, $\tilde{F}_3 = -Pb\tilde{j}$ *(A.25)*

Resultant vector between the resultant force vector and the centroid of the beam,

$$\tilde{r}_3 = -\left[x - \left(x_2 + \frac{b}{2}\right)\right]\tilde{\imath} + \left[T - \frac{T_o}{2}\right]\tilde{j} \quad \textit{(A.26)}$$

Bending Moment,

$$M_3 = \tilde{k} \cdot \left(\tilde{r}_3 \times \tilde{F}_3\right) \quad \textit{(A.27)}$$

Substituting equation *(A.21) and (A.22)* in *(A.23)* we have,

$$M_{3=} Pb\left(x - x_2 - \frac{b}{2}\right) \quad \textit{(A.28)}$$

Bending Moment at Section (4):

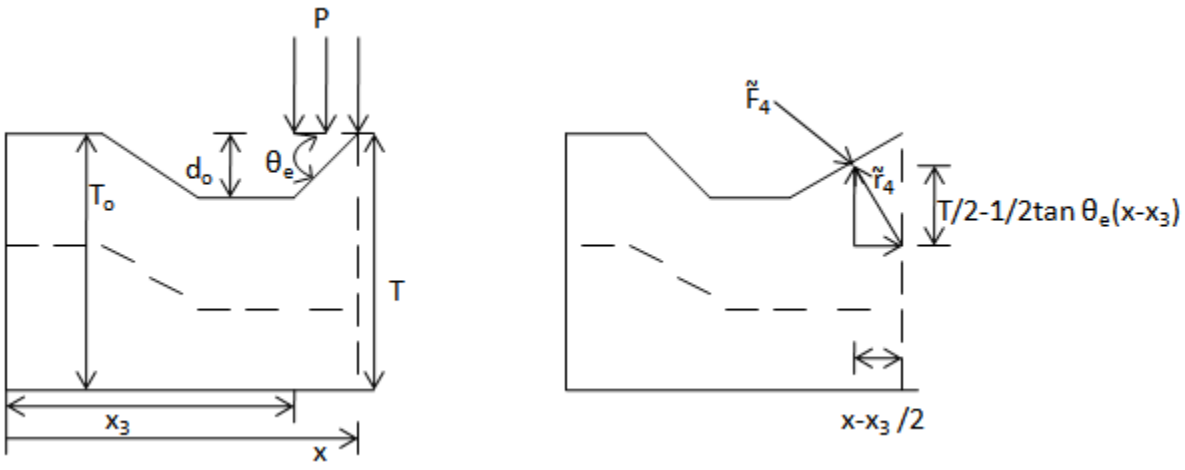

Figure 4.7: Bending Moment at Section (4)

Resultant force vector, $$\tilde{F}_4 = -P\frac{(x-x_3)}{\cos\theta_e}\tilde{n}_e \quad (A.29)$$

Unit vector normal to the contracting surface is given by,

$$\tilde{n}_e = \cos\theta_e\,\tilde{j} - \sin\theta_e\tilde{\imath} \quad (A.30)$$

Substituting equation *(A.30)* in *(A.29)*,

$$\tilde{F}_4 = -P\frac{(x-x_3)}{\cos\theta_e}(\cos\theta_e\,\tilde{j} - \sin\theta_e\tilde{\imath}) \quad (A.31)$$

Resultant vector between the resultant force vector and the centroid of the beam,

$$\tilde{r}_4 = -\left(\frac{x-x_3}{2}\right)\tilde{\imath} + \frac{1}{2}(T_o - d_o)\tilde{j} \quad (A.32)$$

Bending Moment,

$$M_4 = \tilde{k}\cdot\left(\tilde{r}_4 \times \tilde{F}_4\right) \quad (A.33)$$

Substituting equation *(A.31) and (A.32)* in *(A.33)* we have,

$$M_{4=}\frac{1}{2}P(x-x_3)[(x-x_3)+(T_o-d_o)\tan\theta_e] \qquad (A.34)$$

Considering any Section after Section (4):

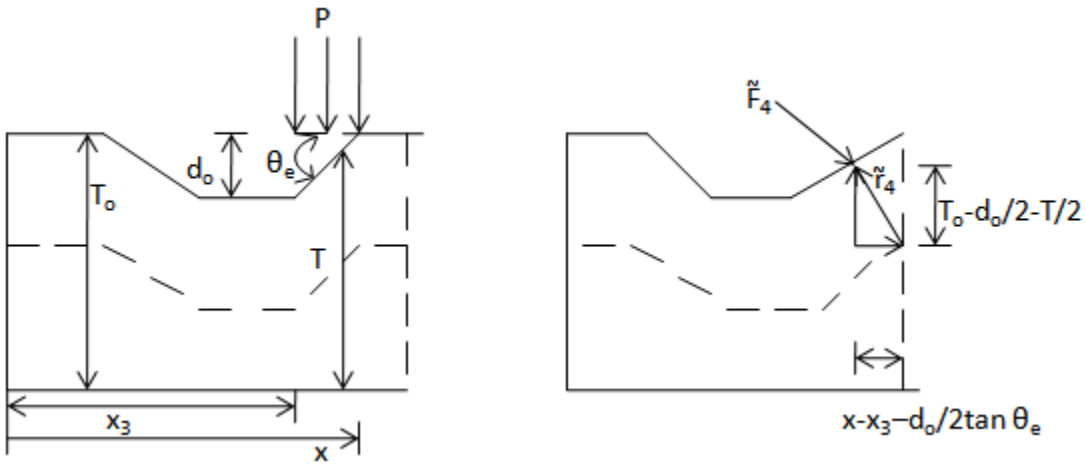

Figure A.8: Bending Moment after Section (4)

Resultant force vector, $$\tilde{F}_4 = -P\frac{d_o}{\sin\theta_e}(\cos\theta_e\,\tilde{j} - \sin\theta_e\tilde{i}) \qquad (A.35)$$

Resultant vector between the resultant force vector and the centroid of the beam,

$$\tilde{r}_4 = -\left[x - \left(x_3 + \frac{1}{2}\frac{d_o}{\tan\theta_e}\right)\right]\tilde{\imath} + \left\{T_o - \left(\frac{d_o}{2} + \frac{T}{2}\right)\right\}\tilde{j} \qquad (A.36)$$

Bending Moment,

$$M_4 = \tilde{k}\cdot\left(\tilde{r}_4 \times \tilde{F}_4\right) \qquad (A.37)$$

Substituting equation *(A.35) and (A.36)* in *(A.37)* we have,

$$M_{4=} Pd_o\left\{\frac{1}{\tan\theta_e}\left[x - x_3 - \left(\frac{1}{2}\frac{d_o}{\tan\theta_e}\right)\right] - \left[T_o - \frac{d_o}{2} - \frac{T}{2}\right]\right\} \qquad (A.38)$$

Bending Moment at Section (5):

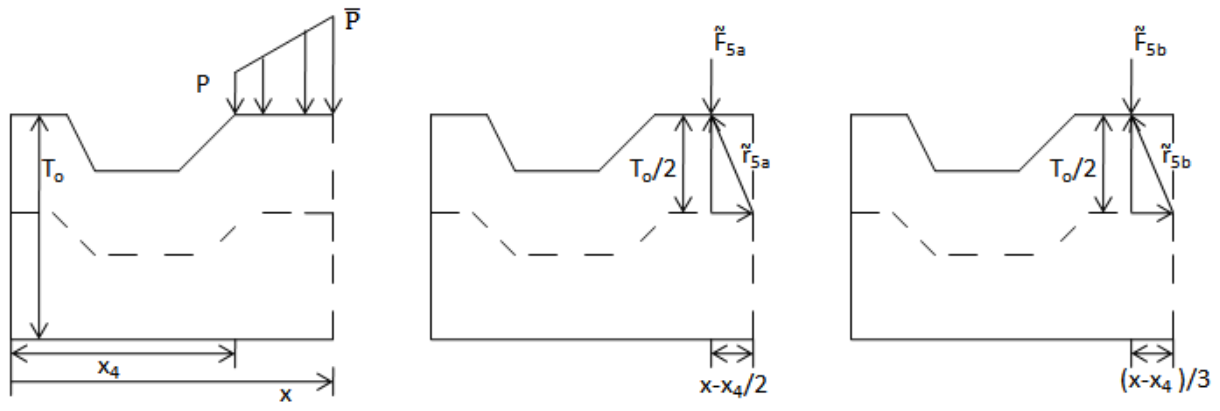

Figure A.9: Bending Moment at Section (5)

Part (a)

Resultant force vector, $$\tilde{F}_{5a} = -\frac{1}{2l_i}(\bar{P} - P)(x - x_4)^2\tilde{j} \quad (A.39)$$

Resultant vector between the resultant force vector and the centroid of the beam,

$$\tilde{r}_{5a} = -\frac{(x-x_4)}{3}\tilde{\imath} + \frac{T_o}{2}\tilde{j} \quad (A.40)$$

Bending Moment,

$$M_{5a} = \tilde{k} \cdot \left(\tilde{r}_{5a} \times \tilde{F}_{5a}\right) \quad (A.41)$$

Substituting equation *(A.39) and (A.40)* in *(A.41)* we have,

$$M_{5a=}\frac{1}{6l_i}(\bar{P} - P)(x - x_4)^3 \quad (A.42)$$

Part (b)

Resultant force vector, $$\tilde{F}_{5b} = -P(x - x_4)\tilde{j} \quad (A.43)$$

Resultant vector between the resultant force vector and the centroid of the beam,

$$\tilde{r}_{5b} = -\frac{(x-x_4)}{2}\tilde{\imath} + \frac{T_o}{2}\tilde{\jmath} \qquad (A.44)$$

Bending Moment,

$$M_{5b} = \tilde{k} \cdot \left(\tilde{r}_{5b} \times \tilde{F}_{5b}\right) \qquad (A.45)$$

Substituting equation *(A.43) and (A.44)* in *(A.45)* we have,

$$M_{5b=} \frac{P}{2}(x - x_4)^2 \qquad (A.46)$$

Total bending moment,

$$M_5 = M_{5a} + M_{5b} \qquad (A.47)$$

$$M_5 = \frac{P}{2l_i}(x - x_4)^2 \left[l_i - \frac{(x-x_4)}{3}\right] + \frac{P_i}{6l_i}(x - x_4)^3 \qquad (A.48)$$

Considering any Section after Section (5):

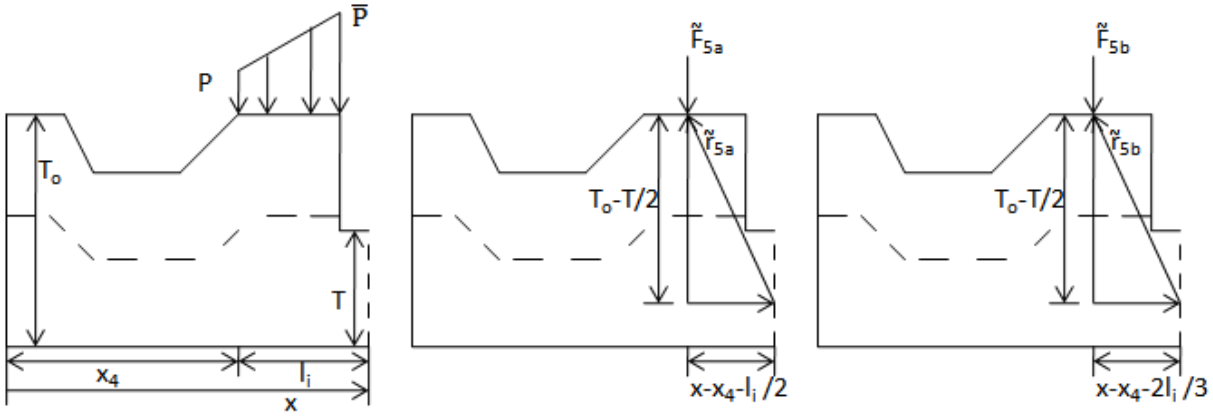

Figure A.10: Bending Moment after Section (5)

Part (a):

Resultant force vector, $$\tilde{F}_{5a} = -\frac{1}{2}\,(\bar{P} - P) l_i \tilde{j} \qquad (A.49)$$

Resultant vector between the resultant force vector and the centroid of the beam,

$$\tilde{r}_{5a} = -\left(x - x_4 - \frac{2}{3} l_i\right)\tilde{\imath} + \left(T_o - \frac{T}{2}\right)\tilde{j} \qquad (A.50)$$

Bending Moment,

$$M_{5a} = \tilde{k} \cdot \left(\tilde{r}_{5a} \times \tilde{F}_{5a}\right) \qquad (A.51)$$

Substituting equation *(A.49) and (A.50)* in *(A.51)* we have,

$$M_{5a=}\, \frac{l_i}{2}(\bar{P} - P)\left(x - x_4 - \frac{2}{3} l_i\right) \qquad (A.52)$$

Part (b)

Resultant force vector $$\tilde{F}_{5b} = -P l_i \tilde{j} \qquad (A.53)$$

Resultant vector between the resultant force vector and the centroid of the beam,

$$\tilde{r}_{5b} = -\left(x - x_4 - \frac{1}{2}l_i\right)\tilde{\imath} + \left(T_o - \frac{T}{2}\right)\tilde{\jmath} \qquad (A.54)$$

Bending Moment,

$$M_{5b} = \tilde{k} \cdot \left(\tilde{r}_{5b} \times \tilde{F}_{5b}\right) \qquad (A.55)$$

Substituting equation *(A.53) and (A.54)* in *(A.55)* we have,

$$M_{5b=} P l_i \left(x - x_4 - \frac{1}{2}l_i\right) \qquad (A.56)$$

Total bending moment,

$$M_5 = M_{5a} + M_{5b} \qquad (A.57)$$

$$M_5 = \frac{Pl_i}{2}\left(x - x_4 - \frac{1}{3}l_i\right) + \frac{\bar{P}l_i}{2}\left(x - x_4 - \frac{2}{3}l_i\right) \qquad (A.58)$$

Bending Moment at Section (6):

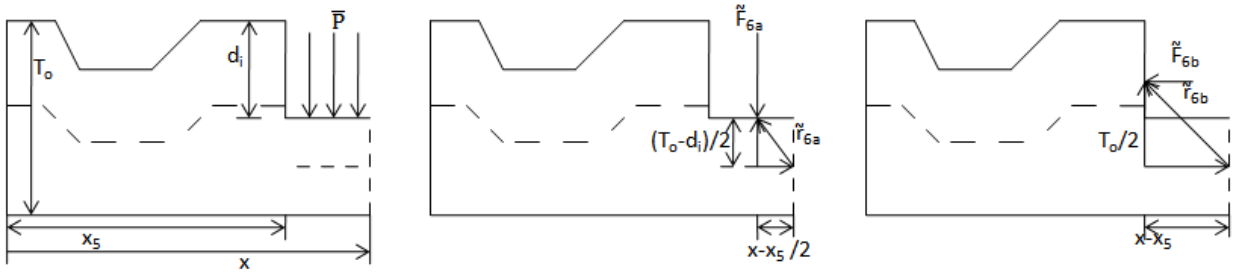

Figure A.11: Bending Moment at Section (6)

Part (a):

Resultant force vector, $$\tilde{F}_{6a} = -\bar{P}(x - x_5)\tilde{j} \quad (A.59)$$

Resultant vector between the resultant force vector and the centroid of the beam,

$$\tilde{r}_{6a} = -\frac{1}{2}(x - x_5)\tilde{\imath} + \frac{(T_o - d_i)}{2}\tilde{j} \quad (A.60)$$

Bending Moment,

$$M_{6a} = \tilde{k} \cdot (\tilde{r}_{6a} \times \tilde{F}_{6a}) \quad (A.61)$$

Substituting equation *(A.59) and (A.60)* in *(A.61)* we have,

$$M_{6a=} \frac{\bar{P}}{2}(x - x_5) \quad (A.62)$$

Part (b):

Resultant force vector, $$\tilde{F}_{6b} = -\bar{P}d_i\tilde{j} \quad (A.63)$$

Resultant vector between the resultant force vector and the centroid of the beam,

$$\tilde{r}_{6b} = -(x - x_5)\tilde{\imath} + \frac{T_o}{2}\tilde{\jmath} \qquad (A.64)$$

Bending Moment,

$$M_{6b} = \tilde{k} \cdot \left(\tilde{r}_{6b} \times \tilde{F}_{6b}\right) \qquad (A.65)$$

Substituting equation *(A.63) and (A.64)* in *(A.65)* we have,

$$M_{6b=} \frac{\bar{P} T_o d_i}{2} \qquad (A.66)$$

Total bending moment,

$$M_6 = M_{6a} + M_{6b} \qquad (A.67)$$

$$M_6 = \frac{\bar{P}}{2}[(x - x_5) + T_o d_i] \qquad (A.68)$$

Appendix B

B1: Couette Flow in Slots

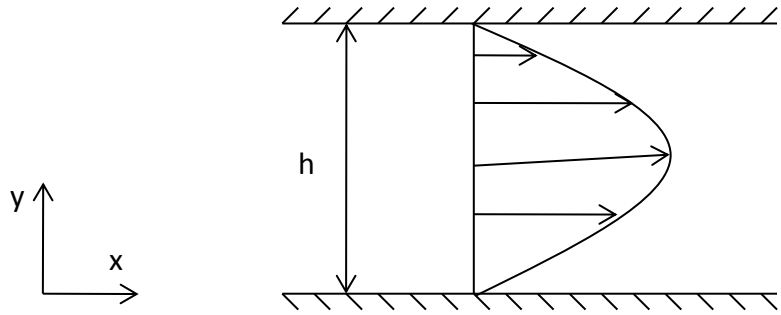

Figure B.1: Flow in Slot

Simplified Navier Stokes equation is given by,

$$-\frac{dp}{dx} + \mu \frac{d^2u}{dy^2} = 0 \qquad (B.1)$$

Integrating above equation twice with respect to dy,

$$\frac{dp}{dx}\frac{y^2}{2} = \mu u + C_1 y + C_2 \qquad (B.2)$$

where C_1 and C_2 are constants.

Applying the boundary conditions: at y=0; u=0 and at y=h; u=0 to equation *(B.2*) we get,

$$C_1 = \frac{dp}{dx}\frac{h}{2} \qquad (B.3)$$

$$C_2 = 0 \qquad (B.4)$$

Substituting equations *(B.3)* and *(B.4)* in *(B.2),*

$$u = \frac{1}{2\mu}\frac{dp}{dx}(y^2 - hy) \qquad (B.5)$$

To obtain pressure gradient,

$$\int_0^h u\, dy = q \qquad (B.6)$$

Substituting equation *(B.5)* in *(B.6) we have,*

$$\frac{dp}{dx} = -\frac{12\mu q}{h^3} \qquad (B.7)$$

B2: Linearized Pressure in the Slots

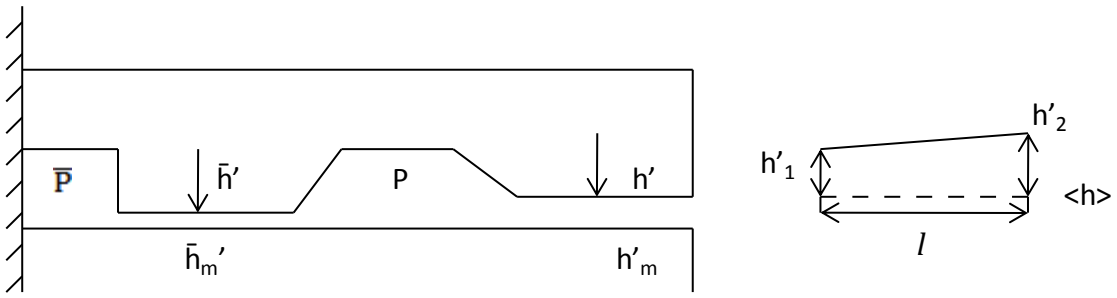

Figure B.2: Side View of a Coating Die

Assuming deflection in the slots to be linear the distorted outer slot height is given by,

$$h = < h > + h' \qquad (B.8)$$

where, $h' = h'_1 + (h'_2 - h'_1)\frac{x}{l}$ *(B.9)*

From equation *(B.7)*

$$f(h) = \frac{1}{h^3} \qquad (B.10)$$

$$f(< h >) = \frac{1}{<h>^3} \qquad (B.11)$$

Differentiating equation *(B.11)* with respect to h=<h>,

$$\frac{df(<h>)}{dh}_{@h=<h>} = -\frac{3}{<h>^4} \qquad (B.12)$$

Using Taylor series expansion for local linearization,

$$f(h) \approx f(< h >) + \frac{df(<h>)}{dh}_{@h=<h>} (h - < h >) \qquad (B.13)$$

Substituting equations *(B.8)*, *(B.11)* and *(B.12)* in *(B.13)*,

$$f(h) \approx \frac{1}{<h>^3} - \frac{3}{<h>^4} h' \qquad (B.14)$$

Substituting equation *(B.14)* and *(B.9)* in the pressure gradient in slot equation *(B.7)* we have,

$$\frac{dP}{dx} = -\frac{12\mu q}{<h>^3}\left[1 - \frac{3\left[h_1^{'} + (h_2^{'} - h_1^{'})\frac{x}{l}\right]}{<h>}\right] \qquad (B.15)$$

Integrating equation (B.15) with respect to x and applying the boundary conditions at x=*l*; P=0, pressure at x=0 we have pressure across the outer slot,

$$P = \frac{12\mu ql}{<h>^3}\left[1 - \frac{3h_m^{'}}{<h>}\right] \text{ where, } h_m^{'} = \frac{(h_1^{'} + h_2^{'})}{2} \qquad (B.16)$$

Similarly, pressure across the inner slot is given by,

$$\bar{P} = P + \frac{12\mu\bar{q}\bar{l}}{<\bar{h}>^3}\left[1 - \frac{3\bar{h}_m^{'}}{<\bar{h}>}\right] \text{ where, } \bar{h}_m^{'} = \frac{(\bar{h}_1^{'} + \bar{h}_2^{'})}{2} \qquad (B.17)$$

Therefore, under the assumption of a linear variation in slot height, the pressure drop across the slot can be expressed in terms of the deflection at the center of the slot.

Appendix C

C1: Shape Factor of a Circular Pipe

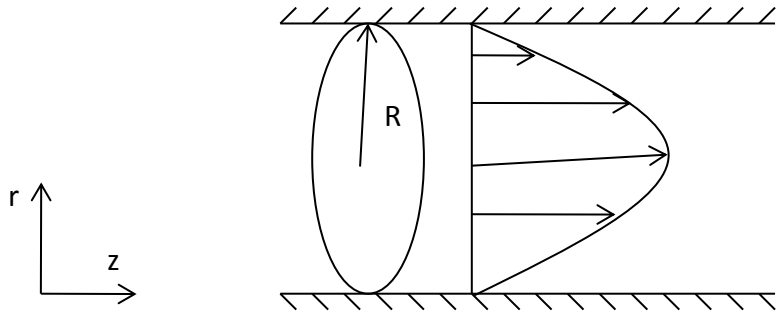

Figure C.1: Flow in a Circular Pipe

Pressure gradient along the circular pipe is given by,

$$-\frac{dp}{dz} = \frac{\mu Q}{\lambda_c {A_c}^2} \qquad (C.1)$$

where λ_c is called the shape factor because its value depends on the geometric shape of the conduit.

Let us consider the fluid in the cylinder between r and r+Δr from the line down the middle. The pressure force maintaining the fluid motion is given by,

$$\text{Net pressure force} = \frac{\Delta p}{l} 2\pi r \Delta r \qquad (C.2)$$

Balanced force equation is,

$$\frac{\Delta p}{l} 2\pi r \Delta r = 2\pi (r + \Delta r)\mu \frac{dv}{dr}(r + \Delta r) - 2\pi r \mu \frac{dv}{dr} r \qquad (C.3)$$

Dividing the above equation by 2π and rearranging,

$$\frac{d}{dr}\left(r \frac{dv}{dr}\right) = \frac{\Delta p}{\mu l} r \qquad (C.4)$$

Differentiating equation *(C.4*) twice with respect to r and applying the boundary conditions at constant C=0, r=R; v(r) =0 we get,

$$v(r) = \frac{\Delta p}{\mu l}\frac{\left(R^2 - r^2\right)}{4} \qquad (C.5)$$

Total flow rate,

$$Q = \int_0^R 2\pi r\, v(r) dr \qquad (C.6)$$

Substituting equation *(C.5)* in *(C.6)* and integrating with respect to r,

$$-\frac{\Delta p}{l} = \frac{\mu Q}{\frac{1}{8\pi}{A_c}^2} \text{ where, } {A_c}^2 = \pi r^2 \qquad (C.7)$$

Comparing equations *(C.1)* and *(C.7)*, the shape factor is given by

$$\lambda_c = \frac{1}{8\pi} = 0.039788735 \qquad (C.8)$$

The circular shape gives the highest possible shape factor and therefore the lowest pressure gradient. However, a circular shape is rarely used in coating dies based on other considerations such as wanting the entire cavity in a single bar.

C2: Continuity Equation at the Inner and Outer Cavities and Slots

The flow in the inner cavity is both in the transverse as well as in the longitudinal direction as shown in figure C.2.

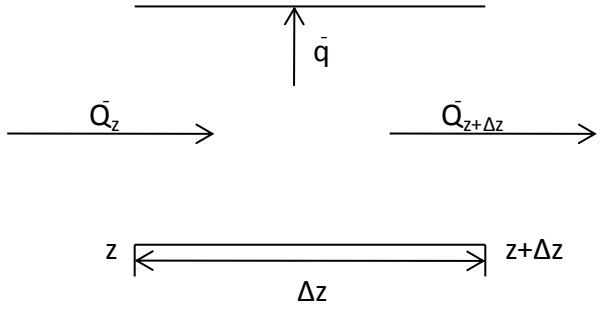

Figure C.2: Continuity at the Inner Cavity and Slot

The balanced volumetric flow rate equation at the inner cavity and slot is given by,

$$\bar{Q}_{z+\Delta z} = \bar{Q}_z - \bar{q}\Delta z \qquad (C.9)$$

Rearranging the above equation we obtain the continuity equation at the inner cavity and slot as,

$$\frac{d\bar{Q}}{dz} = -\bar{q} \qquad (C.10)$$

The outer cavity flow is similar to the inner cavity flow direction and in addition to this it also has the fluid entering it from the inner slot as seen in figure C.3.

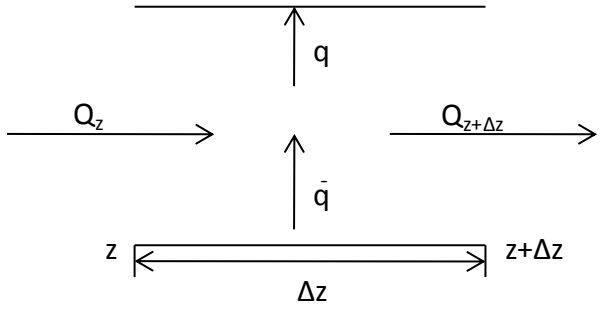

Figure C.3: Continuity at the Outer Cavity and Slot

The balanced volumetric flow rate equation at the outer cavity and slot is given below.

$$Q_{z+\Delta z} - Q_z = \bar{q}\Delta z - q\Delta z \qquad (C.11)$$

Rearranging and substituting equation *(C.9)* in *(C.11)* we obtain the continuity equation at the outer cavity and slot as,

$$\frac{d\bar{Q}}{dz} + \frac{dQ}{dz} = -q \qquad (C.12)$$

C3: Deflection and Flow Coupled Equation for Inner Cavity

The first of the four equations for coupled flow and deflection follows from the flow equation for the inner cavity.

Flow along the inner cavity is given by,

$$-\frac{d\bar{P}}{dz} = \frac{\mu\bar{Q}}{\bar{\lambda}[\bar{A}(z)]^2} \qquad (C.13)$$

Flow along the outer cavity is given by,

$$-\frac{dP}{dz} = \frac{\mu Q}{\lambda A^2} \qquad (C.14)$$

Continuity equation at inner cavity and slot,

$$\bar{q} = -\frac{d\bar{Q}}{dz} \qquad (C.15)$$

Differentiating equation *(C.15)* with respect to z,

$$\frac{d\bar{q}}{dz} = -\frac{d^2\bar{Q}}{dz^2} \qquad (C.16)$$

Pressure in the inner slot from equation *(B.17)*,

$$\bar{P} = \frac{12\mu\bar{q}\bar{l}}{<\bar{h}>^3}\left[1 - \frac{3\bar{h}'_m}{<\bar{h}>}\right] + P \qquad (C.17)$$

Differentiating equation *(C.17)* with respect to z,

$$\frac{d\bar{P}}{dz} - \frac{dP}{dz} = \frac{12\mu\bar{l}}{<\bar{h}>^3}\frac{d\bar{q}}{dz}\left[1 - \frac{3\bar{h}'_m}{<h^->}\right] + \frac{12\mu\bar{q}\bar{l}}{<\bar{h}>^3}\left[-\frac{3}{<\bar{h}>}\frac{d\bar{h}'_m}{dz}\right] \qquad (C.18)$$

Substituting equation *(C.13)*, *(C.14)*, *(C.15)* and *(C.16)* in *(C.18)*,

$$-\frac{\mu\bar{Q}}{\bar{\lambda}[\bar{A}(z)]^2} + \frac{\mu Q}{\lambda A^2} = -\frac{12\mu\bar{l}}{<\bar{h}>^3}\frac{d^2\bar{Q}}{dz^2}\left[1 - \frac{3\bar{h}'_m}{<\bar{h}>}\right] + \frac{12\mu\bar{l}}{<\bar{h}>^3}\frac{d\bar{Q}}{dz}\left[\frac{3}{<\bar{h}>}\frac{d\bar{h}'_m}{dz}\right] \qquad (C.19)$$

Dividing equation (C.19) by $\frac{12\mu}{<h^{-}>^3}$

$$\frac{<\bar{h}>^3}{12}\left[\frac{\bar{Q}}{\bar{\lambda}[\bar{A}(z)]^2}+\frac{Q}{\lambda A^2}\right]=-\bar{l}\frac{d^2\bar{Q}}{dz^2}\left[1-\frac{3\bar{h}_m'}{<h^{-}>}\right]+\bar{l}\frac{d\bar{Q}}{dz}\left[\frac{3}{<\bar{h}>}\frac{d\bar{h}_m'}{dz}\right] \qquad (C.20)$$

C4: Deflection and Flow Coupled Equation for Outer Cavity

The second of the four equations for coupled flow and deflection follows from the flow equation for the outer cavity.

Flow in the outer cavity is given by,

$$-\frac{dP}{dz} = \frac{\mu Q}{\lambda A^2} \qquad (C.21)$$

Continuity equation at outer cavity and slot is,

$$q = -\frac{d\bar{Q}}{dz} - \frac{dQ}{dz} \qquad (C.22)$$

Differentiating equation *(C.22)* with respect to z,

$$\frac{dq}{dz} = -\frac{d^2\bar{Q}}{dz^2} - \frac{d^2Q}{dz^2} \qquad (C.23)$$

Pressure in the outer slot from equation *(B.16)*,

$$P = \frac{12\mu ql}{<h>^3}\left[1 - \frac{3h'_m}{<h>}\right] \qquad (C.24)$$

Differentiating equation *(C.24)* with respect to z,

$$\frac{dP}{dz} = \frac{12\mu l}{<h>^3}\left[\frac{dq}{dz}\left(1 - \frac{3h'_m}{<h>}\right) - \frac{3q}{<h>}\frac{dh'_m}{dz}\right] \qquad (C.25)$$

Substituting equation *(C.21)*, *(C.22)* and *(C.23)* in *(C.25)*

$$\frac{12\mu l}{<h>^3}\left[\left(-\frac{d^2\bar{Q}}{dz^2} - \frac{d^2Q}{dz^2}\right)\left(1 - \frac{3h'_m}{<h>}\right) + \left(-\frac{d\bar{Q}}{dz} - \frac{dQ}{dz}\right)\left(-\frac{3}{<h>}\frac{dh'_m}{dz}\right)\right] + \frac{Q\mu}{\lambda A^2} = 0 \qquad (C.26)$$

Dividing equation *(C.26)* by $\frac{12\mu l}{<h>^3}$ we have,

$$\left(-\frac{d^2\bar{Q}}{dz^2} - \frac{d^2Q}{dz^2}\right)\left(1 - \frac{3h'_m}{<h>}\right) + \left(-\frac{d\bar{Q}}{dz} - \frac{dQ}{dz}\right)\left(-\frac{3}{<h>}\frac{dh'_m}{dz}\right) + \frac{Q<h>^3}{12l\lambda A^2} = 0 \qquad (C.27)$$

Appendix D

D1: Dimensionless Quantities and Groups:

Dimensionless variable for inner slot height is given by,

$$\bar{H}' = \frac{\bar{h}'_m}{<\bar{h}>} \qquad (D.1)$$

$$\bar{h}'_m =< \bar{h} > \bar{H}' \qquad (D.1a)$$

Dimensionless variable for outer slot height is given by,

$$H' = \frac{h'_m}{<h>} \qquad (D.2)$$

$$h'_m =< h > H' \qquad (D.2a)$$

Dimensionless variable for volumetric flow rate in inner cavity,

$$f = \frac{\bar{Q}}{<q>L} \qquad (D.3)$$

Dimensionless variable for volumetric flow rate in inner cavity,

$$g = \frac{Q}{<q>L} \qquad (D.4)$$

Dimensionless variable for inner cavity area,

$$a = \frac{\bar{A}}{\bar{A_o}} \qquad (D.5)$$

Dimensionless variable for cavity length,

$$\xi = \frac{z}{L} \qquad (D.6)$$

Dimensionless inner cavity group is given by,

$$\epsilon = \frac{<\bar{h}>^3 L^2}{12\bar{\lambda}\bar{l}\bar{A}_o{}^2} \qquad (D.7)$$

Dimensionless outer cavity group is given by,

$$s = \frac{<h>^3 L^2}{12\lambda l A^2} \qquad (D.8)$$

Dimensionless slot group is given by,

$$r = \frac{<\bar{h}>^3 l}{<h>^3 l^-} \qquad (D.9)$$

Dividing equation *(D.1)* by *(D.6)*,

$$\frac{\bar{H}'}{\xi} = \frac{\bar{h}'_m L}{<h>z} \qquad (D.10)$$

Differentiating equation *(D.10)* with respect to z,

$$\frac{d\bar{h}'_m}{dz} = \frac{<h>}{L}\frac{d\bar{H}'}{d\xi} \qquad (D.11)$$

Dividing equation *(D.2)* by *(D.6)*,

$$\frac{H'}{\xi} = \frac{h'_m L}{<h>z} \qquad (D.12)$$

Differentiating equation *(D.12)* with respect to z,

$$\frac{dh'_m}{dz} = \frac{<h>}{L}\frac{dH'}{d\xi} \qquad (D.13)$$

Dividing equation *(D.3)* by *(D.6)*,

$$\frac{f}{\xi} = \frac{\bar{Q}}{<q>z} \qquad (D.14)$$

Differentiating equation *(D.14)* with respect to z,

$$\frac{d\bar{Q}}{dz} = < q > \frac{df}{d\xi} \qquad (D.15)$$

Differentiating equation *(D.15)* with respect to z,

$$\frac{d^2\bar{Q}}{dz^2} = \frac{<q>}{L}\frac{d^2f}{d\xi^2} \qquad (D.16)$$

Dividing equation *(D.4)* by *(D.6)*,

$$\frac{g}{\xi} = \frac{Q}{<q>z} \qquad (D.17)$$

Differentiating equation *(D.17)* with respect to z,

$$\frac{dQ}{dz} = < q > \frac{dg}{d\xi} \qquad (D.18)$$

Differentiating equation *(D.18)* with respect to z,

$$\frac{d^2Q}{dz^2} = \frac{<q>}{L}\frac{d^2g}{d\xi^2} \qquad (D.19)$$

D2: Coupled Inner Cavity Dimensionless Equation

Deflection and flow coupled equation for inner cavity is from equation *(C.20)*,

$$\frac{<\bar{h}>^3}{12}\left[\frac{\bar{Q}}{\bar{\lambda}\bar{A}^2}+\frac{Q}{\lambda A^2}\right]=-\bar{l}\frac{d^2\bar{Q}}{dz^2}\left[1-\frac{3\bar{h}_m'}{<\bar{h}>}\right]+\bar{l}\frac{d\bar{Q}}{dz}\left[\frac{3}{<\bar{h}>}\frac{d\bar{h}_m'}{dz}\right] \qquad (D.20)$$

Rearranging equation *(D.13)*,

$$-\frac{<\bar{h}>L^2}{12\bar{\lambda}\bar{l}{\bar{A}_o}^2}\frac{\bar{Q}\bar{l}{\bar{A}_o}^2}{L^2\bar{A}^2}+\frac{<\bar{h}>^3\bar{l}}{<h>^3\bar{l}}\frac{<h>^3L^2}{12\lambda lA^2}\frac{Q\bar{l}}{L^2}+\bar{l}\frac{d^2\bar{Q}}{dz^2}\left[1-\frac{3\bar{h}_m'}{<h^->}\right]-\bar{l}\frac{d\bar{Q}}{dz}\left[\frac{3}{<\bar{h}>}\frac{d\bar{h}_m'}{dz}\right] \qquad (D.21)$$

Substituting equations *(D.1), (D.3), (D.4), (D.5), (D.7), (D.8), (D.9), (D.11), (D.15), (D.16)* in *(D.21)*,

$$-\frac{\epsilon f<q>\bar{l}}{La^2}+\frac{rsg<q>\bar{l}}{L}+\frac{<q>\bar{l}}{L}\frac{d^2f}{d\xi^2}[1-3\bar{H}']-\frac{<q>\bar{l}}{L}3\frac{df}{d\xi}\frac{d\bar{H}\prime}{d\xi}=0 \qquad (D.22)$$

Dividing equation *(D.15)* by $\frac{<q>\bar{l}}{L}$,

$$-\frac{\epsilon f}{a^2}+rsg+\frac{d^2f}{d\xi^2}[1-3\bar{H}']-3\frac{df}{d\xi}\frac{d\bar{H}\prime}{d\xi}=0 \qquad (D.23)$$

D3: Coupled Outer Cavity Dimensionless Equation

Deflection and flow coupled equation for outer cavity from equation *(C.27)*,

$$\left(-\frac{d^2\bar{Q}}{dz^2}-\frac{d^2Q}{dz^2}\right)\left(1-\frac{3h'_m}{<h>}\right)+\left(-\frac{d\bar{Q}}{dz}-\frac{dQ}{dz}\right)\left(-\frac{3}{<h>}\frac{dh'_m}{dz}\right)+\frac{Q<h>^3}{12l\lambda A^2}=0 \qquad (D.24)$$

Substituting equations *(D.2), (D.4), (D.8), (D.13), (D.15), (D.16), (D.18), (D.19),* in *(D.24)*

$$-\frac{<q>}{L}\left[\frac{d^2f}{d\xi^2}+\frac{d^2g}{d\xi^2}\right][1-3H']+<q>\left[\frac{df}{d\xi}+\frac{dg}{d\xi}\right]\left[\frac{3}{L}\frac{dH'}{d\xi}\right]+\frac{sg<q>}{L}=0 \qquad (D.25)$$

Dividing equation *(D.25)* by$\frac{<q>}{L}$,

$$\left[\frac{d^2f}{d\xi^2}+\frac{d^2g}{d\xi^2}\right][1-3H']-3\frac{dH'}{d\xi}\left[\frac{df}{d\xi}+\frac{dg}{d\xi}\right]-sg=0 \qquad (D.26)$$

D4: Linearized Dimensionless Inner and Outer Cavity Equations about Perfect Flow

Flow in inner cavity can be represented as,

$$f = \bar{f} + f' \qquad (D.27)$$

where f' represents a small departure.

Perfect flow distribution in inner cavity is given by,

$$\bar{f} = 1 - \xi \qquad (D.28)$$

Substituting equation *(D.28)* in *(D.27)*,

$$f = (1 - \xi) + f' \qquad (D.29)$$

Differentiating equation *(D.29)* with respect to ξ,

$$\frac{df}{d\xi} = -1 + \frac{df'}{d\xi} \qquad (D.30)$$

Differentiating equation *(D.30)* with respect to ξ,

$$\frac{d^2f}{d\xi^2} = \frac{d^2f'}{d\xi^2} \qquad (D.31)$$

Flow in outer cavity can be represented as,

$$g = 0 + g' \qquad (D.32)$$

where g' represents a small departure. When there is perfect flow from the inner slot there is no flow along the outer cavity.

Differentiating equation *(D.32)* with respect to ξ,

$$\frac{dg}{d\xi} = \frac{dg'}{d\xi} \qquad (D.33)$$

Differentiating equation *(D.33)* with respect to ξ,

$$\frac{d^2g}{d\xi^2} = \frac{d^2g'}{d\xi^2} \qquad (D.34)$$

Dimensionless equation for inner cavity is,

$$-\frac{\epsilon f}{a^2} + rsg + \frac{d^2 f}{d\xi^2}[1 - 3\bar{H}'] - 3\frac{df}{d\xi}\frac{d\bar{H}\prime}{d\xi} = 0 \qquad (D.35)$$

Substituting equations *(D.29), (D.30), (D.31), (D.32)* in *(D.35),*

$$-\frac{\epsilon[(1-\xi)+f']}{a^2} + rsg' + \frac{d^2 f'}{d\xi^2}[1 - 3\bar{H}'] + 3\frac{d\bar{H}\prime}{d\xi} - 3\frac{df\prime}{d\xi}\frac{d\bar{H}\prime}{d\xi} = 0 \qquad (D.36)$$

Ignoring smaller term we have linearized coupled dimensionless equation for inner cavity as,

$$-\frac{\epsilon[(1-\xi)+f']}{a^2} + rsg' + \frac{d^2 f'}{d\xi^2}[1 - 3\bar{H}'] + 3\frac{d\bar{H}\prime}{d\xi} = 0 \qquad (D.37)$$

Dimensionless equation for outer cavity is,

$$\left[\frac{d^2 f}{d\xi^2} + \frac{d^2 g}{d\xi^2}\right][1 - 3H'] - 3\frac{dH'}{d\xi}\left[\frac{df}{d\xi} + \frac{dg}{d\xi}\right] - sg = 0 \qquad (D.38)$$

Substituting equations *(D.30), (D.31), (D.32), (D.33), (D.34)* in *(D.38),*

$$\left[\frac{d^2 f\prime}{d\xi^2} + \frac{d^2 g\prime}{d\xi^2}\right][1 - 3H'] - 3\frac{dH'}{d\xi}\left[\left(-1 + \frac{df\prime}{d\xi}\right) + \frac{dg\prime}{d\xi}\right] - sg' = 0 \qquad (D.39)$$

$$\frac{d^2 f\prime}{d\xi^2} + \frac{d^2 g\prime}{d\xi^2} - 3H'\frac{d^2 f\prime}{d\xi^2} - 3H'\frac{d^2 g\prime}{d\xi^2} + 3\frac{dH'}{d\xi} - 3\frac{dH'}{d\xi}\frac{df\prime}{d\xi} - 3\frac{dH'}{d\xi}\frac{dg\prime}{d\xi} - sg' = 0 \qquad (D.40)$$

Ignoring smaller terms we have linearized coupled dimensionless equation for outer cavity as,

$$\frac{d^2 f\prime}{d\xi^2} + \frac{d^2 g\prime}{d\xi^2} + 3\frac{dH'}{d\xi} - sg' = 0 \qquad (D.41)$$

Appendix E

E1: Dimensionless Coupled Deflection and Flow Equations for Inner Slot

The third of the four equations for coupled flow and deflection follows from the flow equation for the inner slot.

Characteristic inner slot pressure is given by,

$$\bar{P}_c = \frac{12\mu\bar{l}<q>}{<\bar{h}>^3} \qquad (E.1)$$

Substituting equation *(D.15)* in *(C.10)*, the continuity equation for inner cavity and slot we have,

$$\bar{q} = -< q > \frac{df}{d\xi} \qquad (E.2)$$

Inner slot pressure is,

$$\bar{P} = P + \frac{12\mu\bar{q}\bar{l}}{<\bar{h}>^3}\left[1 - \frac{3\bar{h}'_m}{<\bar{h}>}\right] \qquad (E.3)$$

Substituting equations *(D.1)*, *(E.1)*, *(E.2)* in equation *(E.3)*,

$$\bar{P} = P - \bar{P}_c \frac{df}{d\xi}[1 - 3\bar{H}'] \qquad (E.4)$$

Substituting equation *(D.30)*, in *(E.4)* and ignoring smaller terms,

$$\bar{P} = P + \bar{P}_c\left[1 - 3\bar{H}' - \frac{df'}{d\xi}\right] \qquad (E.5)$$

E2: Dimensionless Coupled Deflection and Flow Equations for Outer Slot

The last of the four equations for coupled flow and deflection follows from the flow equation for the outer slot.

Characteristic outer slot pressure is given by,

$$P_c = \frac{12\mu l<q>}{<h>^3} \qquad (E.6)$$

Substituting equations *(D.15)* and *(D.18)* in *(C.12)*, the continuity equation for outer cavity and slot we have,

$$q = -<q>\left[\frac{df}{d\xi} + \frac{dg}{d\xi}\right] \qquad (E.7)$$

Outer slot pressure is,

$$P = \frac{12\mu q l}{<h>^3}\left[1 - \frac{3h'_m}{<h>}\right] \qquad (E.8)$$

Substituting equations *(D.2)*, *(E.6)*, and *(E.7)* in *(E.8)*,

$$P = -P_c\left[\frac{df}{d\xi} + \frac{dg}{d\xi}\right][1 - 3H'] \qquad (E.9)$$

Substituting equation *(D.30)*, and *(D.33)* in *(E.4)* and ignoring smaller terms,

$$P = -P_c\left[1 - 3H' - \frac{df'}{d\xi} - \frac{dg'}{d\xi}\right] \qquad (E.10)$$

Inner slot deflection is given by,

Appendix F

F1: Two-Dimensional Finite Element Analysis due to Pressure Loading using ANSYS

1. Preferences → Structural
2. Preprocessor → Element type → Add/Edit/Delete → Add → Solid → 8 node PLANE 82 Options → Element Behavior → Plane Strain
3. Material Properties → Material Models → Structural → Linear → Elastic → Isotropic →

Young’s Modulus EX=190GPa

Poisson’s Ratio PRXY=0.3

4. Modeling → Create → Key points (KP)

   At (z=0 mm)

   KP1: 0,0,0,

   KP2: 0,0.01,0,

   KP3: 0.025,0.01,0,

   KP4: 0.025,0.03,0,

   KP5: 0.05,0.03,0,

   KP6: 0.06732,0.02,0,

   KP7: 0.08423,0.02,0,

   KP8: 0.09,0.03,0,

   KP9: 0.1,0.03,0,

   At (z=500 mm)

   KP1: 0,0,0,

   KP2: 0,0.01268,0,

   KP3: 0.02165,0.01268,0,

   KP4: 0.02165,0.03,0,

   KP5: 0.04665,0.03,0,

   KP6: 0.06397,0.02,0,

   KP7: 0.08088,0.02,0,

   KP8: 0.08665,0.03,0,

   KP9: 0.09665,0.03,0,

   At (z=1000 mm)

   KP1: 0, 0, 0

   KP2: 0, 0.01586,0

   KP3: 0.01768, 0.01586,0

   KP4: 0.01768, 0.03,0,

   KP5: 0.04268, 0.03,0

KP6: 0.06, 0.02,0

KP7: 0.0769, 0.02,0

KP8: 0.08267, 0.03,0

KP9: 0.09267, 0.03,0

Create → Lines →Lines → Straight Lines → through key points

L1: 1, 2

L2: 2, 3

L3: 3, 4

L4: 4, 5

L5: 5, 6

L6: 6, 7

L7: 7, 8

L8: 8, 9

L9: 9, 10

L10: 10, 11

Create → Areas →Arbitrary → By Lines

A1: L1, L2, L3, L4, L5, L6, L7, L8, L9, L10

5. Meshing → Mesh Tool → Fine (1) → Mesh → Pick Areas
6. Loads-> Define Loads → Apply→ Structural →Displacement → on lines → All DOF → 0

   Pressure: Inner Cavity → 500000 Pa

   Inner Slot → 500000 to 100000 Pa

   Outer Cavity → 100000 Pa

   Outer Slot → 100000 to 0 Pa
7. Solution → Solve → Current LS
8. Post Processor → Plot Results→ Contour Plot→ Nodal Solution→ Vector Sum Displacement.

F2: Two-Dimensional Finite Element Analysis due to Thermal Loading using ANSYS

1. Preferences → Thermal
2. Preprocessor → Element type → Add → Solid → PLANE 77
   Options → Element Behavior → Plane Strain
3. Material Properties → Material Models → Thermal
   Thermal Conductivity→50 W/mK
   Coefficient of thermal expansion→20E-06 m/m^{o}C
4. Modeling → Create → Key points (KP)
   KP1: 0, 0, 0
   KP2: 0, 0.01586,0
   KP3: 0.01768, 0.01586,0
   KP4: 0.01768, 0.03,0,
   KP5: 0.04268, 0.03,0
   KP6: 0.06, 0.02,0
   KP7: 0.0769, 0.02,0
   KP8: 0.08267, 0.03,0
   KP9: 0.09267, 0.03,0
   Create → Lines →Lines → Straight Lines → through key points
   L1: 1, 2
   L2: 2, 3
   L3: 3, 4
   L4: 4, 5
   L5: 5, 6
   L6: 6, 7
   L7: 7, 8
   L8: 8, 9
   L9: 9, 10
   L10: 10, 11
   Create → Areas →Arbitrary → By Lines
   A1: L1, L2, L3, L4, L5, L6, L7, L8, L9, L10
5. Meshing → Mesh Tool → Fine (1) → Mesh → Pick Areas

Loads→ Define Loads → Apply→ Thermal →On Lines

Insulated on the sides

Ambient temperature 20^{o}C on the bottom surface

Fluid temperature 22^{o}C on the top surface

6. Solution → Solve → Current LS
7. Preferences → Structural and thermal
8. Preprocessor → Element type→ Switch element type→ Thermal to Structural
9. Material Properties → Material Models → Structural → Linear → Elastic → Isotropic

   Young's Modulus EX=190GPa

   Poisson's Ratio PRXY=0.3
10. Loads→ Define Loads → Apply→ Structural

    Cantilevered on the left edge

    Thermal loading from thermal analysis results
11. Solution → Solve → Current LS
12. Post Processor → Plot Results→ Contour Plot→ Nodal Solution→ Vector Sum Displacement.

Appendix H

H1: Modeling of the Three-Dimensional Coating Die Using Pro-Engineer 4.0

1. Start Pro-Engineer Wildfire 4.0 and set the working directory.
2. Select new file and name the model. This file will be saved in .prt format.
3. Select blend protrusion tool and then the sketching tool icon. This will switch the screen to sketcher mode. Click the reference plane marked as right.
4. Draw the tapered coating die model on this plane at the center in two dimensional. This figure will have an inner cavity depth and width of 20 and 25 mm respectively and a working length of 100 mm. Use the toggle tool which will make the figure1 inactive. Draw the second figure with inner cavity depth and width of 17.32 mm and 21.65 mm respectively and a working length of 96.65 mm. Repeat the toggle step and draw the third figure which will have inner cavity depth and width of 14.14 mm and 17.68 mm respectively and a working length of 92.68 mm.
5. Next enter the distance of the figure 2 from figure 1 and figure 3 from figure 2. Pro-E will then model a straightly blended three dimensional linearly tapered coating die model.
6. The three-dimensional model is then saved in IGES format in order to import it into ANSYS to carry out the three-dimensional finite element analysis.

H2: Three-Dimensional Finite Element Analysis of the Coating Die Using ANSYS 12.0

1. File → Import the IGES file from Pro-E
2. Preferences → Structural
3. Preprocessor → Element type → Add/Edit/Delete → Add → Solid → tetra 10 node 92
4. Material Properties → Material Models → Structural → Linear → Elastic → Isotropic →
   Young's Modulus EX=190GPa
   Poisson's Ratio PRXY=0.3
5. Meshing → Mesh Tool → Fine (1) → Mesh → Pick All
6. Loads-> Define Loads → Apply→ Structural → Displacement on inner cavity edge → on areas → All DOF → 0
   Symmetric boundary condition on area at the die center

Pressure Loadings on areas:

Inner Cavity → 500000 Pa

Inner Slot → 350000 Pa

Outer Cavity → 100000 Pa

Outer Slot → 50000 Pa

7. Solution → Solve → Current LS
8. Post Processor → Plot Results→ Contour Plot→ Nodal Solution→ Vector Sum Displacement.